Geomorphology 273 (2016) 116–133

Contents lists available at ScienceDirect

Geomorphology

journal homepage: www.elsevier.com/locate/geomorph

Spatial distribution of thermokarst terrain in Arctic Alaska

L.M. Farquharson [a,*], D.H. Mann [a], G. Grosse [b], B.M. Jones [c], V.E. Romanovsky [d,e]

[a] Department of Geosciences, University of Alaska Fairbanks, Fairbanks, AK, USA
[b] Alfred Wegener Institute Helmholtz Centre for Polar and Marine Research, Potsdam, Germany
[c] U.S. Geological Survey, Alaska Science Center, Anchorage, AK, USA
[d] Geophysical Institute, University of Alaska Fairbanks, Fairbanks, AK, USA
[e] Tyumen State Oil and Gas University, Tyument Oblast, 625000 Tyumen, Russia

ARTICLE INFO

Article history:
Received 11 April 2016
Received in revised form 3 August 2016
Accepted 3 August 2016
Available online 7 August 2016

Keywords:
Thermokarst
Thaw
Arctic
Landform mapping

ABSTRACT

In landscapes underlain by ice-rich permafrost, the development of thermokarst landforms can have drastic impacts on ecosystem processes and human infrastructure. Here we describe the distribution of thermokarst landforms in the continuous permafrost zone of Arctic Alaska, analyze linkages to the underlying surficial geology, and discuss the vulnerability of different types of landscapes to future thaw. We identified nine major thermokarst landforms and then mapped their distributions in twelve representative study areas totaling 300-km^2. These study areas differ in their geologic history, permafrost-ice content, and ground thermal regime. Results show that 63% of the entire study area is occupied by thermokarst landforms and that the distribution of thermokarst landforms and overall landscape complexity varies markedly with surficial geology. Areas underlain by ice-rich marine silt are the most affected by thermokarst (97% of total area), whereas areas underlain by glacial drift are least affected (14%). Drained thermokarst-lake basins are the most widespread thermokarst landforms, covering 33% of the entire study region, with greater prevalence in areas of marine silt (48% coverage), marine sand (47%), and aeolian silt (34%). Thermokarst-lakes are the second most common thermokarst landform, covering 16% of the study region, with highest coverage in areas underlain by marine silt (39% coverage). Thermokarst troughs and pits cover 7% of the study region and are the third most prevalent thermokarst landform. They are most common in areas underlain by deltaic sands and gravels (18% coverage) and marine sand (12%). Alas valleys are widespread in areas of aeolian silt (14%) located in gradually sloping uplands. Areas of marine silt have been particularly vulnerable to thaw in the past because they are ice-rich and have low-gradient topography facilitating the repeated development of thermokarst-lakes. In the future, ice-rich aeolian, upland terrain (yedoma) will be particularly susceptible to thaw because it still contains massive concentrations of ground ice in the form of syngenetic ice-wedges that have remained largely intact since the Pleistocene.

1. Introduction

Over the past 14,000 years of post-glacial times, one of the main geomorphic processes operating in Arctic lowlands has been the thaw of ice-rich permafrost leading to the formation of thermokarst topography (Czudek and Demek, 1970; Burn, 1992; Jorgenson et al., 2008a; Grosse et al., 2013). Thermokarst, defined as surface subsidence caused by the melting of massive ice (van Everdingen, 2005), can have pervasive effects on hydrological and ecological processes (Kokelj et al., 2005; Myers-Smith et al., 2007), including the carbon cycle (Grosse et al., 2011). In addition to thermokarst, other thaw-related processes include thermo-erosion (thermal and mechanical erosion by water), thermo-denudation (thaw of sediment subaerially and its subsequent transport by gravity), and thermo-abrasion (the thaw and transport of material by wave action; Are, 1978; Washburn, 1979; van Everdingen, 2005). Here the term thermokarst, refers to the topography and landforms developed after the melting of ground ice by any of the aforementioned processes.

In Arctic Alaska, the region north of the Brooks Range underlain by continuous permafrost (Fig. 1), lowland substrates are commonly ice rich, with total volumetric ice contents ranging from 40 to 90% (Kanevskiy et al., 2013). These high ice contents make the ground vulnerable to thermal disturbance and development of thermokarst terrain. These landforms are diverse: 23 different types have been identified based on topography and hydrology in Arctic Alaska alone (Jorgenson et al., 2008a; Jorgenson, 2013; Kokelj and Jorgenson, 2013).

A number of previous studies have mapped the spatial distribution of thermokarst landforms in arctic lowlands. In Canada, these include thermokarst-lakes (Côté and Burn, 2002; Olthof et al., 2015), active-layer detachment slides (Lewkowicz and Harris, 2005;

* Corresponding author.
E-mail address: lmfarquharson@alaska.edu (L.M. Farquharson).

http://dx.doi.org/10.1016/j.geomorph.2016.08.007
0169-555X/

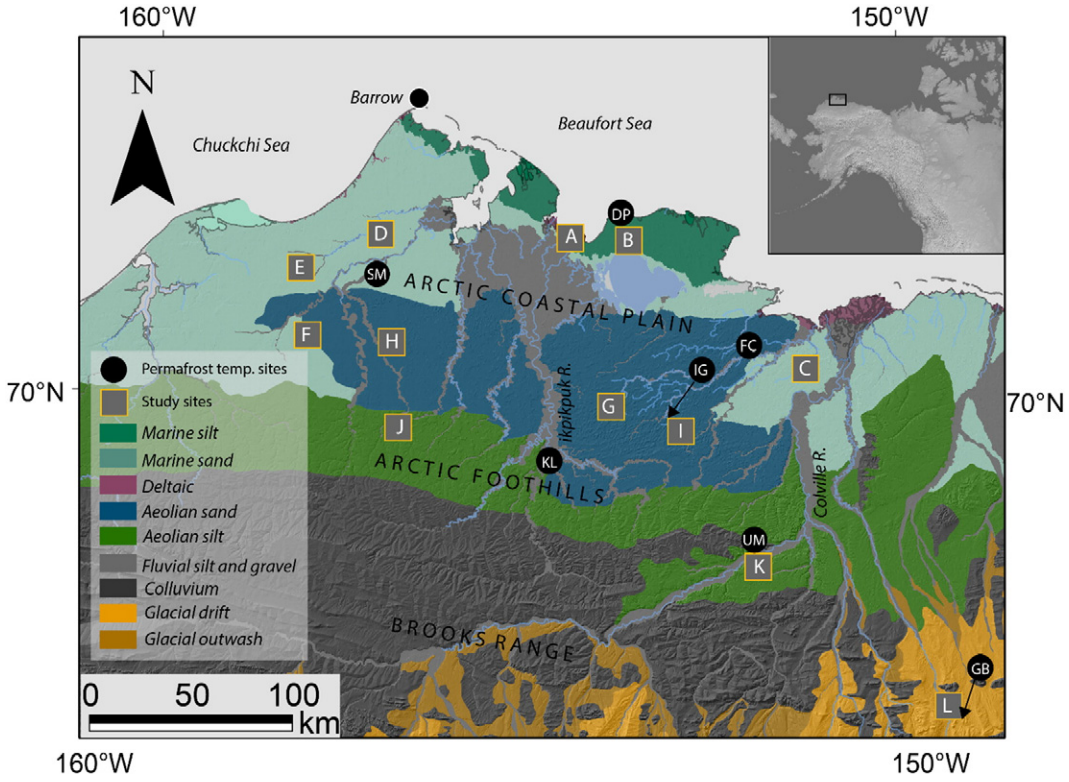

Fig. 1. The study area in northern Alaska. Squares indicate locations of 5 × 5 km areas where we mapped thermokarst landforms. Surficial geology base map was modified from Jorgenson et al. (2008b). Permafrost borehole sites are marked as black circles: DP: Drew Point, SM: South Meade, FC: Fish Creek, IG: Inigok, KL: Koluktak, UM: Umiat, GB: Galbraith.

Lamoureux and Lafreniére, 2009), retrogressive thaw slumps (Lantuit and Pollard, 2008; Lantz and Kokelj, 2008; Kokelj et al., 2009), and degrading ice-wedges (Steedman et al., 2016). In Alaska (Table 2), mapping has focused mainly on the spatial distribution of thermokarst-lakes and drained thermokarst-lake basins (Frohn et al., 2005; Hinkel et al., 2005; Jones et al., 2011; Jones and Arp, 2015) and to a lesser extent beaded streams (Arp et al., 2015), retrogressive thaw slumps (Balser et al., 2014), and ponds formed by degrading ice-wedges (Raynolds et al., 2014; Jorgenson et al., 2015; Liljedahl et al., 2016). In Siberia, Veremeeva and Gubin (2009) identified a number of landscape typologies in the Kolyma River lowlands including upland yedoma and alases. Other mapping in Siberia has quantified thermokarst-lake and drained thermokarst-lake basin distribution in yedoma regions (Grosse et al., 2008; Morgenstern et al., 2011).

The combination of ice-rich permafrost and a rapidly warming climate makes Arctic Alaska an interesting and topical place to study the geomorphic patterns and processes of thermokarst development. Mean annual air temperature (MAAT) at Point Barrow has increased by ~3 °C since 1950 (Wendler et al., 2010), and borehole measurements of ground temperatures indicate permafrost has warmed as much as 4 °C across the region during recent decades (Romanovsky et al., 2010, 2015; Smith et al., 2010). Warming over the coming century is expected to be the greatest at high latitudes (Cohen et al., 2014), and MAAT in the Arctic is projected to rise as much as 8.3 °C (IPCC, 2013).

Ongoing warming has already led to a noticeable increase in thermokarst development in some parts of Arctic Alaska (Jorgenson et al., 2006, 2015; Raynolds et al., 2014; Liljedahl et al., 2016), and we know from paleorecords that warming climate can trigger rapid and widespread thawing of permafrost (Mann et al., 2010; Gaglioti et al., 2014). Short-lived ecological disturbances in conjunction with longer-term warming trends can also trigger thermokarst. For example, wildfires are projected to increase in frequency, intensity, and extent in Arctic Alaska as climate warms there (Hu et al., 2015). Burning removes the organic mat that insulates the ground and buffers the permafrost from warming surface conditions (Jones et al., 2015).

To predict landscape-scale responses to ongoing climatic warming in the Arctic, we need to better understand what factors control thermokarst development there. With this goal in mind, we use remotely sensed imagery to map thermokarst landforms and quantitatively characterize how geological substrate and topography interact with the content and structure of ground ice to determine the incidence, morphology, and distribution of thermokarst landforms that have developed in Arctic Alaska in post-glacial times. Our results provide a basis for predicting how thaw-related, geomorphic processes may respond to climate warming during the coming century.

2. Study region

Our 12 study areas are located on the Arctic Coastal Plain, in the Arctic Foothills, and in the Brooks Range (Wahrhaftig, 1965; Fig. 1). We selected these study areas to be representative examples of the landscapes within which they occur. The number of study areas per type of surficial geology corresponds roughly to how widely this geological substrate is distributed in the study region (Fig. 1, Table 1). Detailed mapping was conducted in six types of surficial geologies: aeolian silt, aeolian sand, marine silt, marine sand, glacial drift, and deltaic sand and gravel (Jorgenson et al., 2008b). All of the study areas are underlain by continuous permafrost (Fig. 2). All sites except those in the Brooks Range are in areas that remained unglaciated during the last glacial maximum (ca. 21,000 YBP (years before present). The permafrost temperature data (for the period 1999 to 2011) used in this study were obtained from the U.S. Geological Survey (http://pubs.usgs.gov/ds/812/introduction.html) and the University of Alaska Geophysical Institute Permafrost Laboratory (http://permafrost.gi.alaska.edu/site/gl1; Fig. 2, Table A.2). Permafrost temperature stations (shown in Fig. 1) do not coincide directly with our study areas but are located within the same

Table 1
Percent cover of different types of surficial geology in the study region, the number of surveyed areas mapped, mean slope of these survey areas, and estimated ice content.

Surficial geology	% of study area shown in Fig 1	Polygons mapped	Mean slope (°)	Mean volumetric ice content (%) (Kanevskiy et al., 2013)
Deltaic sands and gravels	2	A	0.04	73
Marine silt	4	B	0.03	86
Marine sand	33	C, D, E, F	0.1	80
Aeolian sand	23	G, H, I	0.1	43
Aeollian silt	35	J, K	0.32	89
Glacial drift	2	L	2.04	No data

surficial geology units. Mean annual (calendar year) values for ground temperature are calculated using mean daily data from each site.

2.1. Arctic Coastal Plain: Deltaic sands and gravels

Deltaic sands and gravels cover 2% of the study region (Fig. 1, Table 1). Representative of these deposits, study area A (Fig. 1) is located on the Ikpikpuk River delta where the surficial geology is characterized by fine-grained, overbank deposits along with two types of channel deposits: sandy riverbed and lateral-accretion deposits (Shur and Jorgenson, 1998). The mean slope of the ground surface on the Ikpikpuk Delta is 0.04° (Table 1, all slope values represent regional mean slope, see Section 3.2). Once delta channels are abandoned, epigenetic and syngenetic permafrost aggrades and ice-wedge polygons form. Total volumetric ice contents in these deposits vary widely but average 70% in areas of syngenetic ice-wedges (Shur and Jorgenson, 1998). The Ikpikpuk delta probably dates to the mid-Holocene when relative sea level stabilized. Most of the delta surface is either barren or vegetated by pioneering herbaceous vegetation such as *Salix alaxensis*, *Salix lanata*, and *Carex aquatilis* (Jorgenson et al., 1998). No permafrost temperature data are available for this surficial geology type.

2.2. Arctic Coastal Plain: Marine silt

Study area B (Fig. 1) is situated on marine silt, which was deposited during the most recent marine transgression affecting the Arctic Coastal Plain during the Simpsonian interstadial ca. 75,000 cal. YBP when relative sea level was ~7 m higher than today (Dinter et al., 1990). Marine silt covers 4% of the overall study region (Fig. 1) and is limited to outer portions of the Arctic Coastal Plain. The land surface here is basically flat with a mean slope of only 0.03° (Table 1). At Drew Point (Fig. 2), permafrost temperatures at 1.2 m depth averaged −8.0 °C between 1999 and 2010 and have increased by 0.6 °C over this period. At marine-silt sites, total volumetric ice content reaches 86% (Kanevskiy

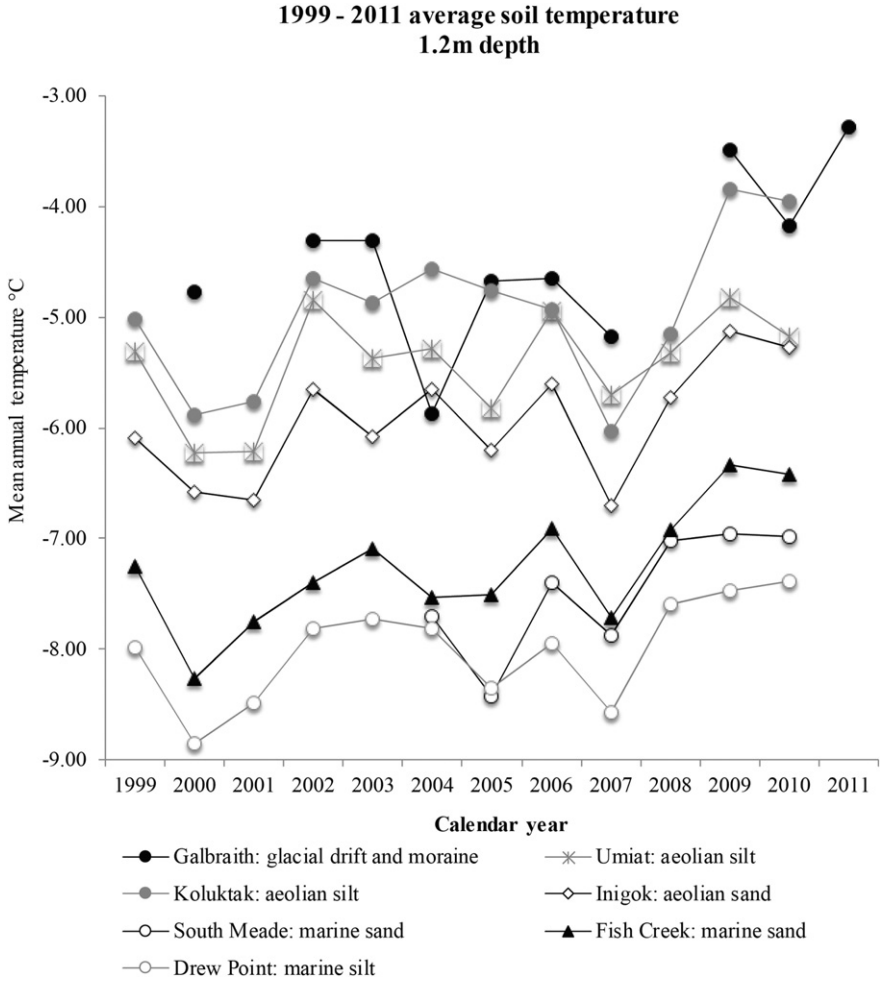

Fig. 2. Mean annual ground temperatures at 1.2 m depth (except for Galbraith, 1.0 m) for calendar years 1999–2011. All data sets acquired from USGS with the exception of Galbraith, which was acquired from the Geophysical Institute Permafrost Laboratory, University of Alaska.

et al., 2013), and vegetation is moist acidic tundra composed of wetland sedges, *Carex aquatilis* and *Eriophorum angustifolium*, and mosses, *Drepanocladus brevifolius*, and *Limprichtia revolvens* (Raynolds et al., 2006).

2.3. Arctic Coastal Plain: Marine sand

Study areas C, D, E, and F are located in areas underlain by marine sand (Fig. 1). In total, marine sand underlies 33% of the study region, and these areas have a mean slope of 0.10° (Table 1). This sand was deposited during multiple marine transgressions of Pleistocene and Pliocene age (Dinter et al., 1990). Permafrost temperatures at 1.2 m depth averaged −7.3 °C between 1999 and 2010 and increased by 0.8 °C during this period (Fig. 2, Fish Creek and South Meade sites). At the marine-sand sites, total volumetric ice content averages 80% (Kanevskiy et al., 2013), and vegetation is moist acidic tundra composed of wetland sedge, *Carex aquatilis* and *Eriophorum angustifolium*, mosses, *Drepanocladus* spp. and *Sphagnum* spp., and dwarf shrubs, *Dryas integrifolia* and *Salix reticulata* (Raynolds et al., 2006).

2.4. Arctic Coastal Plain: Aeolian sand

The aeolian sand sites (G, H, and I; Fig. 1) are located along the southern margin of the Arctic Coastal Plain in the area of the now stabilized Ikpikpuk Sand Sea (Carter, 1981; Galloway and Carter, 1993). Here late Pleistocene and early Holocene deposits of aeolian sand reach up to 30 m in thickness. The former Ikpikpuk Sand Sea is characterized by stabilized longitudinal and parabolic sand dunes covering >15,000-km^2 of the Arctic Coastal Plain. The last period of widespread aeolian activity was 8000–11,000 cal. YBP (Carter, 1981; Dinter et al., 1990). Since this time, reactivation has occurred only intermittently and locally. Altogether, aeolian sand covers 23% of the study region (Fig. 1, Table 1), and the mean slope of the area blanketed by aeolian sand is 0.10° (Table 1). Mean permafrost temperatures at 1.2 m depth in the former sand sea were −5.9 °C between 1999 and 2010, and they increased 0.8 °C during this period (Fig. 2, site Inigok). The average volumetric ice content here reaches 43% (Kanevskiy et al., 2013), which is slightly greater than the typical porosity of frozen sands. At aeolian sand sites, vegetation cover is primarily moist, nonacidic tundra composed of sedge: *Eriophorum vaginatum*, dwarf shrubs, *Ledum palustre*, *Vaccinium vitis-idaea*, *Cassiope tetragona*, and *Rubus chamaemorus*, and mosses, *Sphagnum compactum*, *Aulacomnium turgidum*, and usually lacks any peat accumulation (Raynolds et al., 2006).

2.5. Arctic Foothills: Aeolian silt (yedoma)

Study areas J and K are located in a belt of ice-rich silt (yedoma) lying along the southern margin of the Ikpikpuk Sand Sea and north of previously glaciated terrain (Fig. 1; Shur et al., 2012). Yedoma is organic-rich silt (loess) deposited during the late Pleistocene. It typically contains large, syngenetic ice-wedges (Kanevskiy et al., 2011). In total, yedoma covers 35% of the study region (Fig. 1), and the mean slope of the yedoma zone is 0.32° (Table 1). Mean permafrost temperatures at 1.2 m depth were −5.2 °C between 1999 and 2010, and permafrost temperature increased by as much as 1.0 °C during this period (Fig. 2, sites Koluktak and Umiat). Deposition of yedoma mainly took place during the late Pleistocene, and it accumulated up to 50 m thick in some areas of Beringia (Schirrmeister et al., 2013). Within our study area, yedoma is characterized by a high total volumetric ice content of 89%, mainly because of the presence of syngenetic ice-wedges (Kanevskiy et al., 2011). Vegetation cover is moist acidic tundra characterized by sedges, *Carex bigelowii*, *and Eriophorum angustifolium*, dwarf shrubs, *D*ryas integrifolia and *Salix reticulata*, forbes, *Tephroseris frigida*, and *Eutrema edwardsii*, and mosses, *Drepanocladus brevifolius* and *Distichium capillaceum* (Raynolds et al., 2006).

2.6. Brooks Range: Glacial drift

Study area L is located in the Brooks Range where four glacial advances, the most recent between 24,000 and 17,000 cal. yr BP, have left behind a complex surficial geology (Hamilton, 2003; Fig. 1). In total, glacial drift covers 2% of the study region (Fig. 1), and these areas have a mean slope of 2.04° (Table 1). Permafrost temperatures at 1.0 m depth are the warmest of all the surficial geology types, averaging −4.6 °C for the period 2000 to 2011 (Fig. 2, Galbraith). These ground temperatures increased by 1.5 °C between 2000 and 2011. Thermokarst landforms in this area have developed mainly from the melting of buried glacial ice bodies (Hamilton, 2003), augmented by the melting of Holocene-aged ice wedges. Thermokarst-lakes within this substrate type can also be termed kettle lakes in cases where they formed from the thaw and collapse of buried glacial ice. Vegetation is nonacidic tundra composed of sedges, *Eriophorum vaginatum* and *Carex bigelowii*, dwarf shrubs, *Betula nana*; *Ledum palustre*, *Vaccinium vitis-idaea*, and mosses, *Sphagnum* spp., and *Hylocomium splendens* (Raynolds et al., 2006).

3. Methods

3.1. Definition of thermokarst landforms

We selected study areas of contrasting surficial geology and ground-ice content based on the mapping of Jorgenson et al. (2008b). The study areas are representative of the terrain and surficial geology types occurring in Arctic Alaska.

We mapped nine different thermokarst landforms, all of which are familiar in the periglacial literature (French, 2007; Jorgenson, 2013; Soloviev, 1973), with the exception of flooded ice-wedge polygons and thaw valleys. The landforms in this study are not the only ones existing in Arctic Alaska, but they are the main ones. Five of the thermokarst landforms are large features (>50 m^2): thermokarst-lakes, drained thermokarst-lake basins, alas valleys (Soloviev, 1973; Goudie, 2004), thaw valleys, and retrogressive thaw slumps. Four of the thermokarst landforms are relatively small features (<50 m^2): beaded stream ponds, drained thaw-ponds, thermokarst troughs and pits, and flooded ice-wedge polygons (Fig. 3). Most thermokarst landforms were identified according to the visual characteristics and spatial dimensions described by Jorgenson et al. (2008a) and Jorgenson (2013). Drained thaw-ponds were identified aerially and during field surveys on the basis of pools of standing water, drowned vegetation, and concentric vegetation zonation suggesting variable water levels in the past. We used the descriptions of Soloviev (1973) to identify alas and thaw valleys. We classify alas and thaw valleys together, as they exhibit the same morphology — thermokarst-lake basins connected by valleys or valley-like features — but the term “alas valley” specifically refers to yedoma regions.

3.2. Mapping of thermokarst landforms

Thermokarst landforms (Fig. 3) were mapped in twelve 25-km^2 study areas (Figs. 1, 4). We delineated landforms by manually digitizing features using 2.5-m resolution, false color, infrared, aerial-image orthophotography (July, August 2002–2006) for all sites except L, for which we used 0.3-m resolution World View 2 imagery. An IfSAR DSM (Inferometic Synthetic Aperture Radar Digital Surface Model) was also used for all sites. Raw IfSAR data were collected by Intermap Technologies using a STAR-3i airborne synthetic aperture radar system (high-resolution, single pass) in summers between 2002 and 2006 (Intermap, 2010). IfSAR DSM tiles were used to create a raster mosaic of the study areas with a horizontal resolution of 5 m and a vertical resolution of 1 m. Bluff heights were calculated using the IfSAR DSM. Elevation ranges were assessed for individual landforms within a 50-m buffer around the feature. Slope data were calculated using the Scenarios

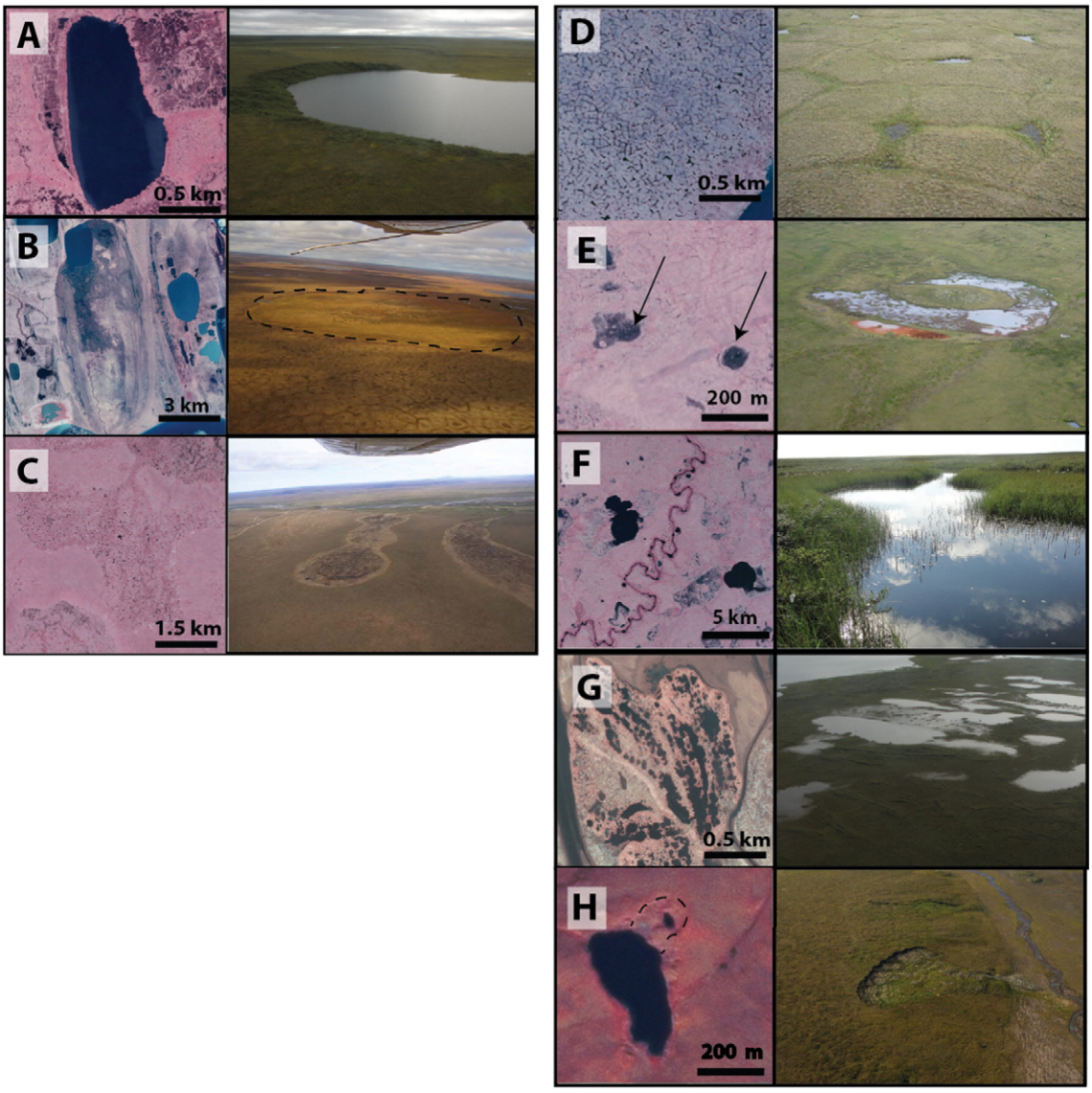

Fig. 3. Mapped landforms in planview (left) and oblique view (right). (A) thermokarst-lake, (B) drained thermokarst-lake basin, (C) alas valley (morphology similar to thaw valley), (D) thermokarst troughs and pits, (E) drained thaw-pond, (F) beaded stream, (G) flooded ice-wedge polygons, (H) retrogressive thaw-slump. Oblique photos are for descriptive purposes and not necessarily from the locations shown in the aerial photos.

Network for Alaska (SNAP) 1-km resolution Alaska slope model (http://ckan.snap.uaf.edu/dataset/slope). To estimate slope angles, we used 1-km resolution slope data, because the 5-m resolution, IfSAR slope data are affected by small-scale topographic features. For water bodies, we used the water and lake/river ice classes used in the National Land Cover Database (Homer et al., 2015), which is based on classification of 2001–2011 Landsat-5 Thematic Mapper data at 30-m resolution, which allows us to map all lakes >1 ha. Landforms were manually digitized in ArcMap v.10.0 (ESRI™) software (see Grosse et al., 2006; Morgenstern et al., 2011) at a scale of 1:2000. Landform metrics data were also calculated using ArcMap. To assess the accuracy of landform mapping, we conducted ground surveys of all 12 study areas in the summer of 2013. Qualitative surveys were conducted on foot, using maps overlain by our landform classification. In addition, all five authors have spent considerable time in the area, conducting geomorphic research, on foot and during low-elevation flight surveys.

We adhered to set rules when mapping complicated landforms. For instance, landform boundaries were manually delineated around clusters of thermokarst troughs and pits and flooded polygons exhibiting similar degradation and ponding characteristics. Beaded streams were digitized as polylines and then buffered with a width of 90 m (Arp et al., 2015) using the buffer analysis tool in ArcGIS. Multi-basin lakes and drained-lake basins were divided into individual lakes when the basins exhibited roughly an hourglass shape indicative of coalescence. In site A (Ikpikpuk Delta), active river channels were masked at the water line and not included in land-cover calculations. Landform density was calculated by counting the number of each landform type present in each study area, then dividing by the area affected by thermokarst.

3.3. Classification of terrain as 'currently active thermokarst' or 'previously active thermokarst'

We used the spectral characteristics of vegetation cover and liquid water to classify thermokarst landforms as either currently active or previously active. In addition, we mapped areas that had no observable thermokarst landforms. Currently thermokarst affected landforms are those under the influence of thermokarst processes at the time of image acquisition. In the case of thermokarst trough and pit zones and thermokarst-lakes, we interpreted the presence of standing water pits and troughs as indicative of active thermokarst, which may lead to underestimating the extent of these features in areas with good

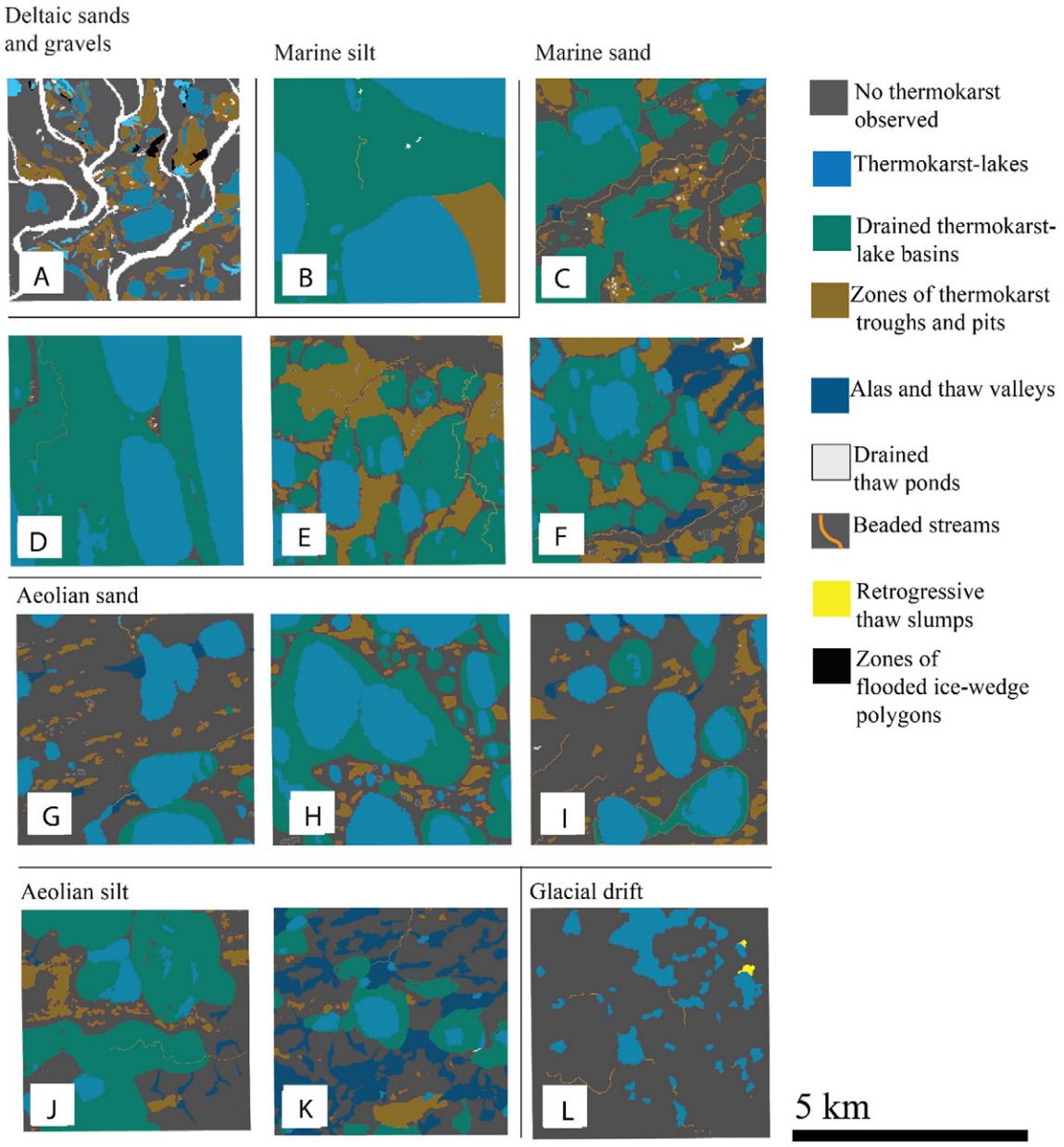

Fig. 4. Mapped areas grouped by surficial geology. Letters correspond to those in Fig. 1.

drainage. In the case of beaded channels, we interpreted the presence of water as a probable indicator of talik (thaw bulb) presence. All alas and thaw valleys had low reflectivity values associated with landscape wetting and/or showed signs of strong ice-wedge degradation and ponding at the head of the channel system.

Currently inactive landforms are those not actively developing at the time of image acquisition. Vegetation cover was used as a key indicator of geomorphic stability. Vegetated retrogressive thaw slump scars were classified as currently inactive thermokarst terrain. Areas classified as non-thermokarst-affected were those where no evidence of either current or past thermokarst activity was detected.

We quantified the extent of repeated ice aggradation and subsequent thaw across the landscape by determining the number of overlapping generations of thermokarst-lakes (Billings and Peterson, 1980; Jones et al., 2012). We mapped the cross-cutting relationships of multiple thermokarst-lakes using the outlines of former basins where they were visible and extrapolating the likely location of lake margins that had been destroyed by subsequent lake generations. To make such extrapolations, we assume these lakes tend to have circular or elliptical shapes.

4. Results

4.1. Distribution of thermokarst landforms in relation to surficial geology

4.1.1. Deltaic sands and gravels

On the Ikpikpuk delta (site A), 37% of the landscape has been affected by thermokarst processes (Figs. 4–6, Table 3). The most widely distributed landforms are thermokarst troughs and pits, which cover 18% of the total area (Fig. 5, Table 3). Individual groupings of thermokarst troughs and pits have an average area of 3.7 ha (Table 4). Small lakes (mean area 8.1 ha; Table 4) cover 13% of the study area. Mean elevation range is 4.7 m (Table 4). This study area has a landform density of 14.5 landforms per km^2 (Fig. 7). No drained thermokarst-lake basins were observed, and all thermokarst landforms observed are currently classified as active (Fig. 6).

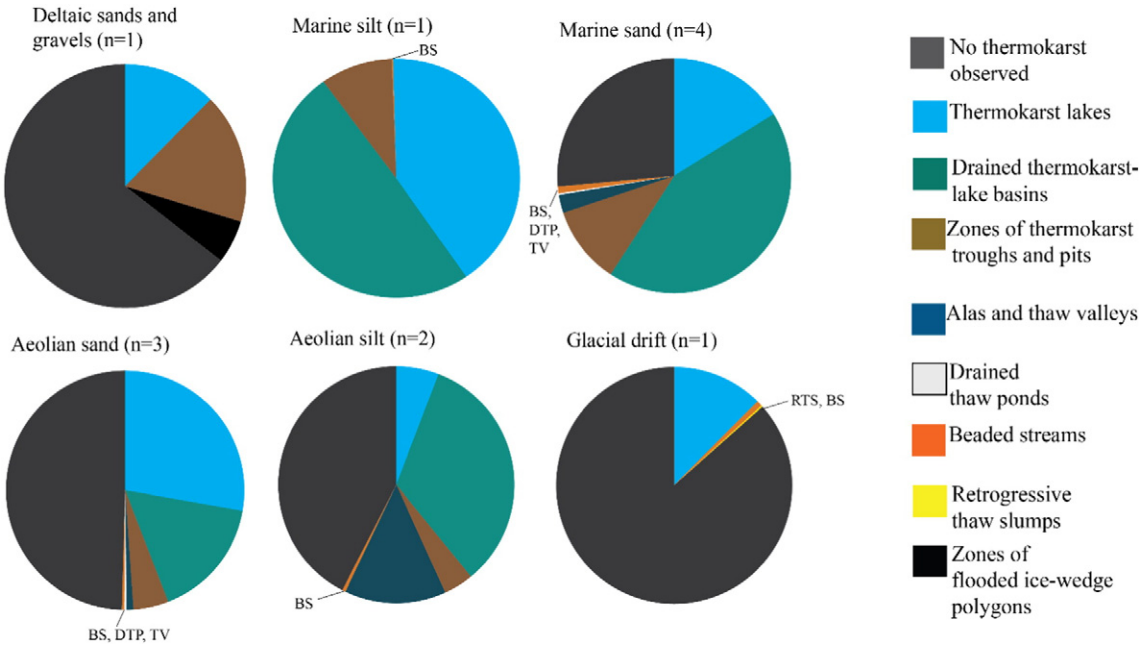

Fig. 5. Distribution of thermokarst landforms in relation to surficial geology. The n values indicate number of study areas underlain by each of the six surficial geology units. BS: beaded stream, DTP: drained thaw pond, TV: thaw valley, RTS: retrogressive thaw slump.

4.1.2. Areas of marine silt

The extent of thaw-affected terrain is greatest on the northern Arctic Coastal Plain where ice-rich marine silt is present (site B). Here, thermokarst has modified 97% of the landscape (Figs. 4 and 6, Table 3). Three percent of the area was unclassified because of the presence of small water bodies <1 ha in size situated within drained thermokarst-lake basins. Drained thermokarst-lake basins and thermokarst-lakes are the dominant thermokarst landforms, covering 48 and 39% respectively of the study area (Fig. 5, Table 3). These basins and lakes have mean surface areas of 232 and 110 ha, respectively (Table 4). Mean bluff height is relatively low for thermokarst-lakes and drained thermokarst-lake basins, only 3.5 and 5.3 m, respectively (Table 4). Up to four generations of drained-lake basins are present in addition to existing thermokarst-lakes (Fig. 8). In this study area, a single zone of thermokarst troughs and pits is perched on an upland area comprising 9% of the total study area. Four types of thermokarst landforms are present, which yields a relatively low landform density of 0.9 per km^2 (Fig. 7). A low landform density combined with a high percentage of thermokarst cover results from few landforms that are relatively large in size. When grouped into currently and previously active landforms, 48% of study area B is comprised of previously active landforms and 48% by currently active landforms (Fig. 6).

4.1.3. Areas of marine sand

Thermokarst processes affect 81% of study areas underlain by marine sand (sites C, D, E, F, Figs. 4–6, Table 3). Drained thermokarst-lake basins cover 47% of the total area, which is similar to their coverage of the marine silt sites (site B, Fig. 4, Table 3). Thermokarst-lakes and drained

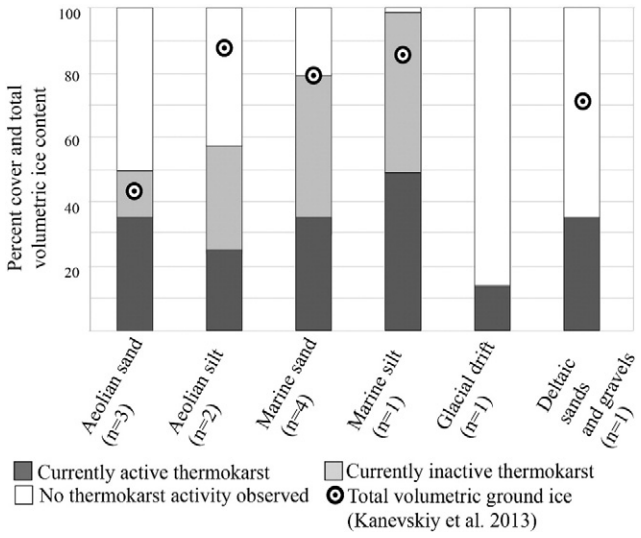

Fig. 6. Relationships between thermokarst, surficial geology, and the amount of ground ice present. No estimates of ground ice are available for the glacial drift area.

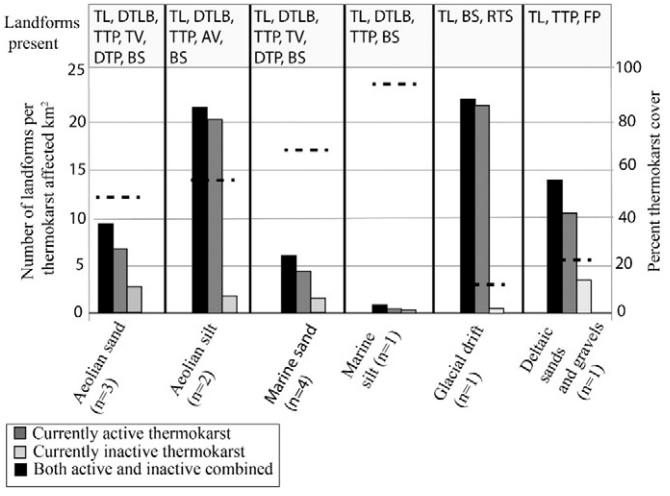

Fig. 7. Relationships between surficial geology, the amount of thermokarst that occurs, and what form this thermokarst takes. Solid bars show the number of individual, thermokarst landforms per km^2 in areas of differing surficial geology. Dotted lines correspond to right-hand axis and indicate what percentage of that type of lithology is or has been affected by thermokarst. TL: thermokarst-lake, DTLB: drained thermokarst-lake basin, TTP: zones of thermokarst troughs and pits, AV: alas valley, TV: thaw valley, DTP: drained thaw ponds, BS: beaded stream, RTS: retrogressive thaw slump, FP: zones of flooded ice-wedge polygons.

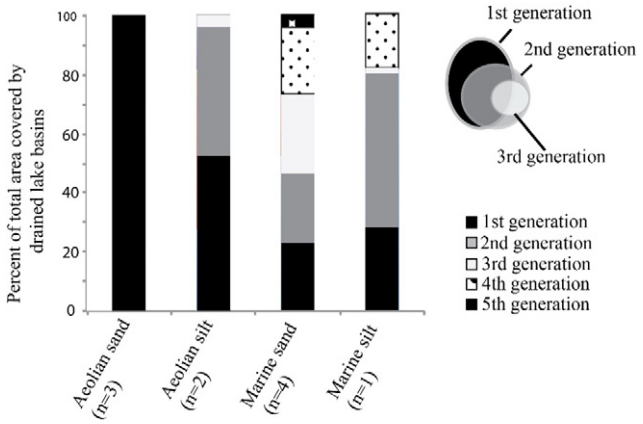

Fig. 8. Number of drained thermokarst-lake generations observed (see example, top right) in areas of differing surficial geology. Study areas L (glacial drift) and A (deltaic sands and gravels) are not shown because no drained thermokarst-lake basins were mapped there.

thermokarst-lake basins have a mean surface area of 33 and 59 ha, respectively (Table 4). Mean bluff heights for drained thermokarst-lake basins and thermokarst-lakes are 5.0 and 2.5 m, respectively. Up to five generations of drained thermokarst-lake basins are present in addition to the existing thermokarst-lakes (Fig. 8). Thermokarst-lakes are less prevalent than drained thermokarst-lake basins, covering only 18% of the total study area, whereas ice-wedge polygon zones account for 12% of the combined marine sand sites (Fig. 5, Table 3). Other landforms include alas valleys (3%), drained thaw-ponds (0.2%), and beaded streams (<1%; Figs. 4 and 5). Once grouped into currently and previously active landforms, 33% of the land surface is currently active, and 48% of the landscape by previously active landforms (Fig. 6). Marine sand exhibits a high diversity of landform, with six types of thermokarst landforms present, including drained thaw-ponds, beaded streams, and thaw valleys, resulting in an average of 5.9 individual landforms per km^2 (Fig. 7).

4.1.4. Aeolian sand

Thermokarst processes affect 50% of study areas located within the former Ikpikpuk Sand Sea (sites G, H, I, Figs. 4–6, Table 3). The most common landforms are thermokarst-lakes (28%) and drained thermokarst-lake basins (16%). Whereas previous studies (Jorgenson and Shur, 2007) suggest non-thermokarst causes of lake initiation, our observations suggest that ice-wedge degradation is an important mechanism in the growth of lakes in the former sand sea.

Areas of aeolian sand, as well as areas of marine sand, have the most diverse geomorphology of any area mapped. In addition to thermokarst-lakes and drained thermokarst-lake basins, four other thermokarst landforms occur: thermokarst troughs and pits, beaded streams, thaw valleys, and drained thaw-ponds. Thermokarst-lakes and drained thermokarst-lake basins cover areas of 38 and 37 ha, respectively (Table 4). The average height of lake bluffs bordering drained thermokarst-lake basins is 7.0 and 9.0 m. Only one generation of drained thermokarst-lake basins occurs in addition to the existing thermokarst-lakes (Fig. 8). Zones of thermokarst troughs and pits cover 5% of aeolian sand areas (Table 3). Beaded streams, thaw valleys, and drained thaw-ponds have similarly limited coverage. In total, 33% of aeolian sand areas are covered by currently active landforms and 17% by previously active landforms (Fig. 6). This leaves some 49% of the landscape that preserves relict, sand-dune landforms and so exhibits no evidence of either past thermokarst processes or ongoing thermokarst activity (Fig. 6).

4.1.5. Areas of aeolian silt

Thermokarst processes have affected ~58% of the landscape in the aeolian silt (yedoma) zone of the Arctic Foothills (sites J and K, Figs. 4–6, Table 3). Drained thermokarst-lake basins are the most widely distributed landform (Fig. 5), covering 34% of the combined study areas (Table 3) with a mean area of 80 ha per individual basin (Table 4). Mean bluff height bordering drained thermokarst-lake basins and thermokarst-lakes is 19.3 and 11.0 m, respectively. Some 24% of the landscape is characterized by currently active landforms and 34% by previously active landforms (Fig. 6). Thermokarst trough and pit zones and beaded streams cover 4 and <1% of the total area, respectively. Zones of aeolian silt show similar landform density to those of glacial drift, with 22 landforms per thaw-affected km^2 (Fig. 7). Up to three generations of drained thermokarst-lake basins occur in addition to extant thermokarst-lakes (Fig. 8). Thermokarst-lakes have a more restricted coverage here than do alas valleys, covering 6 and 14% of sites J and K, respectively (Table 3). Individual alas valleys and thermokarst-lakes have a mean area of 12 ha (Table 4).

4.1.6. Glacial drift

Areas underlain by glacial drift exhibit the lowest percent coverage by thermokarst landforms of any study area, only 14% (site L, Figs. 4–6, Table 3). Within the glacial drift, thermokarst-lakes are the dominant thermokarst landform (Fig. 5), covering 12.6%, with a mean area of 9 ha (n = 35; Table 4). The average bluff height around these lakes is 13.7 m, likely reflecting the presence of massive, buried glacial ice in the area. Thaw slumps (observed only on lake margins; n = 2) and beaded streams (n = 13) account for the remaining thaw-affected area (<1%; Fig. 5). Site L is the only study area where retrogressive thaw slump activity occurs. This study area exhibits high spatial complexity, with 22 landforms per thermokarst-affected kilometer squared (Fig. 7). Because no currently thermokarst affected lake margins were found, we suspect that either the ice bodies bordering lakes in this study area have already melted-out, or that ice-bodies are now protected by a layer of thawed material. Two stabilized retrogressive thaw slumps belong to the category of previously thermokarst affected landforms.

4.2. Distribution of thermokarst landforms on a regional basis

Based on 1528 digitized individual landforms within 12 study areas covering a total of 300-km^2, 63% of the study landscape is currently or has been previously affected by thermokarst processes (Figs. 3 and 4, Table 3). This leaves 37% of the study area as non-thermokarst-affected terrain, much of which is underlain by ice-rich permafrost (Kanevskiy et al., 2013), which implies it is vulnerable to future thaw.

Thermokarst-lakes and drained thermokarst-lake basins are the most numerous and spatially extensive thermokarst landforms across all geological substrates. Drained thermokarst-lake basins cover 33% of the study area, and extant thermokarst-lakes 16%. The third most abundant type of landform are thermokarst troughs and pits, which cover 7% of the total study area. Rarer landforms include alas and thaw valleys (6% cover, mainly observed in regions underlain by aeolian silt/yedoma), drained thaw-ponds (<1% cover), beaded streams (<0.1% cover), retrogressive thaw slumps (<0.1% cover, only observed in areas underlain by glacial drift), and flooded ice-wedge polygons (<1% cover, only observed in areas underlain by deltaic sand and gravel).

In addition to being most numerous, drained thermokarst-lake basins are the thermokarst landforms occupying the greatest mean surface area per individual feature, 62 ha (n = 168). Thermokarst-lakes have the second greatest mean surface area per individual feature, 24 ha (n = 212). The smaller mean size of thermokarst-lakes compared to drained thermokarst-lake basins results from the basins being formed by multiple generations of coalescent, drained lakes. Alas and thaw valleys are the third largest landform with a mean area of 12 ha (n = 88). The landforms with the smallest mean size are drained thaw-ponds (area = 1 ha; n = 110), retrogressive thaw slumps (3 ha; n = 2), zones of thermokarst troughs and pits (3 ha; n = 887), and beaded streams (4.8 ha; n = 37). Mean elevation range of these landforms

varies from 10.7 m (beaded streams) to 2.6 m (drained thaw-ponds). Overall, beaded streams and alas and thaw valleys exhibit the highest mean elevation ranges, 10.7 and 9.0 m, respectively (Table 4).

5. Discussion

5.1. Comparison with previous studies

Overall, our findings are similar to previous mapping efforts of permafrost-affected arctic lowlands. Our cover estimates for thermokarst-lakes and drained thermokarst-lake basins in areas of marine silt and sand align closely with previous results from the Arctic Coastal Plain of Alaska (Frohn et al., 2005; Hinkel et al., 2005; Wang et al., 2012; Jones and Arp, 2015; Table 2). Mapped areas of yedoma areas in the lowlands of northern Siberia exhibit similar coverage by thermokarst-lakes and drained thermokarst-lake basins as our study (Grosse et al., 2006, 2008; Morgenstern et al., 2011; Tables 2 and 3). Although our estimates of percent cover by drained thermokarst-lake basin at aeolian silt sites in the Arctic Foothills (34%) agree with previous studies in this region (Wang et al., 2012), they differ from observations in similar substrates on the northern Seward Peninsula and in the Kolyma lowlands, where the distribution of drained thermokarst-lake basins is much greater, around 75 (Jones et al., 2012) and 61% (Veremeeva and Gubin, 2009) respectively. This difference may be because most thermokarst-lakes on the Seward Peninsula have developed on a flat plain rather than in the foothills. The mean slope for the aeolian silt region of the Arctic Foothills is 0.30° whereas the mean slope on the Seward Peninsula lowlands is only 0.15°, which is similar to areas of marine sand in our study area.

Finally, our results regarding beaded stream distribution generally agree with previous mapping efforts in Arctic Alaska (Jorgenson et al., 2008a, 2008b; Arp et al., 2015). Arp et al. (2015) observed a lower distribution of beaded streams across areas of aeolian sand compared to other surficial geology types on the Arctic Coastal Plain, a pattern also seen in this study. High ground ice content and greater topographic relief probably favor the formation of beaded streams.

5.2. Distribution of landforms

We found that regardless of underlying surficial geology, thermokarst-lake development is the dominant, thermokarst geomorphic process in lowland areas of Arctic Alaska, as mapped at this point in time. Thermokarst-lake development (thermokarst-lakes and drained thermokarst-lake basins combined) has affected 49% of the combined study areas and has been most intense in areas of marine silt and sand (Figs. 4 and 5). These areas typically are underlain by ice-rich permafrost and are relatively flat. In combination, both of these factors are conducive to repeated cycles of thermokarst pit, thermokarst pond and eventual thermokarst-lake, development. In contrast, thermokarst-lakes and drained thermokarst-lake basins are much less abundant in areas underlain by aeolian sand, aeolian silt, glacial drift, or deltaic deposits (Figs. 4 and 5).

Though less widespread, landforms like alas and thaw valleys and thermokarst troughs and pits are important components of Arctic Alaska's landscape. Alas and thaw valleys are largely restricted to areas underlain by aeolian silt, where they cover around 14% of the landscape. In contrast, zones of thermokarst troughs and pits occur in all surficial geological types, albeit at low densities. Altogether, zones of thermokarst troughs and pits cover ~7% of the combined study areas. The only surficial-geology type where they do not occur is in glacial drift. This may result from the pronounced topographic relief there (mean slope there is 2°) that creates good drainage conditions that inhibit extensive ice-wedge polygon pond development. Thermokarst troughs and pits are most extensive in areas underlain by deltaic sands and gravels and marine sands where they cover 18 and 12%, respectively. Though not observed during this study, it is important to note that thermokarst troughs and pits can also form within ancient drained thermokarst-lake basins. Over hundreds to thousands of years, epigenetic ice-wedges form within lacustrine sediments and terrestrial peat, and any disturbance to the ground thermal regime can result in ice-wedge degradation.

Beaded stream channels cover only a small percentage of the landscape regardless of surficial geology (0.6%). Despite their restricted occurrence, beaded streams play an important role in sediment and nutrient transport through tundra watersheds (Arp et al., 2015).

Among the factors controlling the distribution of thermokarst landforms in Arctic Alaska, the two most important are probably the volume of ground ice and the regional drainage gradient. Cryolithology — the amount, structure, and spatial distribution of ice in the ground — strongly influences thermokarst processes (Jorgenson et al., 2008a; French and Shur, 2010). The more ice there is underground, the greater effect its melting has on surface topography. Topography also exerts a very basic control over the development of thermokarst landforms through its effects on surface drainage. For instance, the greater topographic relief of the northern Seward Peninsula compared to the Arctic Coastal Plain probably contributes to differences in the abundances of

Table 2
Previous estimates of coverage by thermokarst landforms in Alaska and Siberia.

Reference	Study area	Surficial geology	TK lake % cover	Drained TK lake % cover	Alas valley % cover	Zones of thermokarst troughs and pits %	Beaded streams % cover
Hinkel et al. (2003)	Barrow Peninsula	Marine silt and marine sand	22	50	–	–	–
Frohn et al. (2005)	Arctic Coastal Plain	Mixed	20	26	–	–	–
Frohn et al. (2005)	Inner Coastal Plain	Aeolian sand	14	22	–	–	–
Frohn et al. (2005)	Outer coastal Plain	Marine sand and silt	22	45	–	–	–
Jones and Arp (2015)	Outer coastal Plain	Marine silt	23	62	–	–	–
Arp and Jones (2009)	Northern Seward Peninsula	Aeolian silt	7	-	–	–	–
Jones et al., 2012	Northern Seward Peninsula	Aeolian silt	-	76	–	–	–
Morgenstern et al., 2011	Lena Delta	Yedoma (similar to aeolian silt)	5.2	20	42.5	–	–
Grosse et al. (2005)	Bykovsky Peninsula	Yedoma (similar to aeolian silt)	10.2	31.2	–	–	–
Grosse et al. (2008)	Bykovsky Peninsula	Yedoma (similar to aeolian silt)	15	–	–	–	–
Grosse et al. (2006)	Laptev Sea region	Yedoma (similar to aeolian silt)	7	–	–	–	–
Grosse et al. (2008)	Cherskii	Yedoma (similar to aeolian silt)	>1	–	–	–	–
Grosse et al. (2008)	SW Lena Delta	Yedoma (similar to aeolian silt)	13	–	–	–	–
Jorgenson et al. (2008a, 2008b)	Continuous permafrost zone, Alaska	Mixed	1.9	7.1	–	2.3	0.4
Veremeeva and Gubin (2009)	Kolyma Lowland	Yedoma (similar to aeolian silt)	–	53.5*	–	8	–

* Existing and drained TK lakes combined.

Table 3
Percent cover of thermokarst landforms according to type of surficial geology; weighted percentages calculated using extent of surficial geology area shown in Fig. 1 and described in Section 2, (TL: thermokarst-lake, DTLB: drained thermokarst-lake basin, TTP: zones of thermokarst troughs and pits, AV: alas valley, TV: thaw valley, DP: drained thaw ponds, BS: beaded stream, FP: zones of flooded ice-wedge polygons, RTS: retrogressive thaw slump).

	Deltaic sand and gravel		Marine silt		Marine sand		Aeolian sand		Aeolian silt		Glacial drift		Whole study region
	% cover of study area	Wtd% cover region	% cover of study area	Wtd% cover region	% cover of study area	Wtd% cover region	% cover of study area	Wtd% cover region	% cover of study area	Wtd% cover region	% cover of study area	Wtd% cover region	Wtd% cover
TL	12.86	0.26	39.41	1.58	17.87	5.90	27.90	6.42	5.89	2.06	12.56	0.25	16.46
DTLB	0.00	0.00	48.42	1.94	47.29	15.61	16.48	3.79	33.55	11.74	0.00	0.00	33.08
TTP	17.73	0.35	9.20	0.37	11.87	3.92	4.79	1.10	4.12	1.44	0.00	0.00	7.18
AV/TV	0.00	0.00	0.00	0.00	2.75	0.91	0.93	0.21	14.03	4.91	0.00	0.00	6.03
DP	0.00	0.00	0.00	0.00	0.24	0.08	0.30	0.07	0.00	0.00	0.00	0.00	0.15
BS	0.00	0.00	0.16	0.01	1.02	0.34	0.33	0.08	0.47	0.16	0.79	0.02	0.60
FP	5.96	0.12	0.00	0.00	0.00	0.00	0.00	0.00	0.00	0.00	0.00	0.00	0.12
RTS	0.00	0.00	0.00	0.00	0.00	0.00	0.00	0.00	0.00	0.00	0.22	0.00	0.00
Total tk (%)	36.55		97.19		81.04		50.73		58.06		13.57		63.26
Total no. tk Cover (%)	63.45		2.81		18.96		49.27		41.94		86.43		36.74

alas valleys compared to thermokarst-lakes in areas of aeolian silt in the two areas. One possible explanation for the low abundance of thermokarst-lakes in the Arctic Foothills is that in aeolian silt areas the average terrain slope is steep enough to facilitate the runoff of meltwater from degrading ice-wedge polygons. Meltwater then becomes channelized instead of ponding and tends to form alas valleys rather than thermokarst-lakes.

Differences in environmental history may also explain some of the variability in thermokarst landforms on different geological substrates in Arctic Alaska. The initiation and expansion of peat occurred across Arctic Alaska and northern Siberia during postglacial times in a time-transgressive fashion (Mann et al., 2002; Macdonald et al., 2006). Earlier peat accumulation in some areas may have formed an insulating layer (Baughman et al., 2015) that shielded the underlying permafrost from later climatic perturbations and subsequent thaw (Gaglioti et al., 2014).

The age of the landscape also influences the distribution of thermokarst landforms. On older surfaces, thermokarst processes have had more time to rework the landscape and, for instance, to cycle through multiple generations of thermokarst-lakes and drained-lake basins (Billings and Peterson, 1980; Jorgenson and Shur, 2007; Fig. 8). Results of this study show that older land surfaces (see Section 2), including areas underlain by marine silt and marine sand, contain the largest landforms: namely, drained thermokarst-lake basins and thermokarst-lakes. In contrast, younger land surfaces like the Ikpikpuk Delta, support less thermokarst activity and possess more abundant, smaller-scale landforms, mainly zones of thermokarst troughs and pits.

Older land surfaces may provide indications about the future, developmental trajectories of younger landscapes. For instance, the relative abundance of thermokarst troughs and pits on young surfaces may represent the initial stage of formation for other thaw-related landforms including thermokarst-lakes (Czudek and Demek, 1970; Farquharson et al., 2016), beaded streams (Arp et al., 2015), and in some cases, thaw-slumps (Burn and Lewkowicz, 1990).

5.3. Landscape vulnerability to future thaw

The vulnerability of permafrost terrain to thaw is mediated by the climate at the ground surface, and the climate of Arctic Alaska is currently changing rapidly. In response, permafrost temperatures are rising in all the surficial geology types we studied (Fig. 2). The fastest rates of warming are in the glacial drift (up to 1.5 °C increase between 2000 and 2011) and in aeolian silt areas (1.1 °C increase between 1999 and 2010). Interestingly, sites with the coldest (−7.4 °C) permafrost are also the most thaw-affected, probably because they are more ice-rich than the warmer (−3.3 °C) permafrost sites. Mean annual air temperature (MAATs) is projected to increase in the Arctic by up to 8.3 °C over the coming century (see IPCC, 2013, Table 22.2), and this will undoubtedly cause further ground temperature warming in Arctic Alaska.

Changing climate is causing an increased frequency of wildland fires in Arctic Alaska (Hu et al., 2015). Fire is a major threat to landscape stability there because it destroys the peat layers that insulate the ground and buffer the underlying permafrost from changes in air temperature (Mack et al., 2011). Removal of these insulating peat layers from terrain underlain by ice-rich permafrost can trigger drastic and widespread thermokarst (Jones et al., 2015). Our finding that areas underlain by aeolian silt contain large areas (43%) not yet affected by thermokarst suggests this surficial geology type possesses a relatively high degree of resistance to thaw. One possible explanation for this resistance is that the higher slope angle of this surficial geology type compared to most others (Table 3) improves drainage conditions and inhibits thermokarst. Alternatively, the presence of extensive areas of non-thaw-affected terrain in yedoma areas may result from an earlier spread of insulating organic soils in post-glacial times, which so far has buffered the underlying permafrost from periods of warm temperature (Mann et al., 2010). If true, this implies that peat-supporting yedoma areas may now be highly vulnerable to extensive thermokarst triggered by more frequent wildland fires.

Two surficial geology types in Arctic Alaska — marine silt, and aeolian silt — have high potentials for severe thermokarst development based on their excess ice contents, and in the case of aeolian silt, the amount of land area not previously affected by thermokarst. What these two surficial geology types have in common is the presence of abundant silt. Silt is well-known for its capacity for holding large amounts of excess ice (Yershov, 1998; French, 2007).

Of the two surficial geology types where future thermokarst can be expected to be most severe, areas underlain by aeolian silt probably have the highest potential because they contain deeply distributed excess ice (Jorgenson et al., 2008b; Kanevskiy et al., 2011, 2013; Fig. 4), and a large proportion (43%) of this surficial geology type has not been previously thermokarst affected. Although areas underlain by marine silt also contain high amounts of excess ice, it is mainly in the form of epigenetic ice-wedges restricted to the upper several meters of the ground. Most of the terrain underlain by marine silt in our study region has already been reworked by thermokarst processes during post-glacial times, and future thermokarst landform development will be constrained to reworking these previously thermokarst-affected areas. These varying magnitudes of potential thermokarst responses are reflected in the depth of thermokarst-related surface settling revealed

by bluff heights. The bluffs bordering drained thermokarst-lake basins in areas underlain by marine silt average only 5.3 m in height, whereas bluffs in areas of aeolian silt where excess ice contents are greater, average 19.3 m high (Table 4).

Table 4
Spatial statistics for each type of landform across the entire study area and within each type of surficial geology, (abbreviations as in Table 3).

	Count	Mean elevation range (m)	Mean area (ha)	Min. area (ha)	Max. area (ha)	Range (ha)	Std (ha)
Entire study area							
TL	212	6.36	24.33	0.09	8.00	559.03	63.52
DTLB	168	6.93	61.69	0.02	864.32	864.31	108.29
TTP	887	-	3.14	0.00	230.04	230.04	14.17
AV/TV	88	8.97	11.89	0.00	77.65	77.64	14.03
DP	110	2.64	1.04	0.00	11.39	11.39	1.93
BS	37	10.67	4.80	0.08	26.53	26.45	6.37
RTS	2		2.77	1.37	4.18	2.81	1.99
FP	24		2.69	0.32	10.73	10.41	2.33
Total #	1528	(Currently active = 1358, Currently inactive = 170)					
Deltaic sands and gravels							
TL	35	4.74	8.08	1.17	105.30	104.13	17.87
DTLB	0	–	0.00	0.00	0.00	0.00	0.00
TTP	111	–	3.69	0.00	62.25	62.25	7.77
TV	0	–	0.00	0.00	0.00	0.00	0.00
DP	20	–	3.32	0.08	11.39	11.30	3.40
BS	0	–	0.00	0.00	0.00	0.00	0.00
FP	24	–	2.69	0.32	10.73	10.41	2.33
Total #	190 (Currently active = 170, Currently inactive = 20)						
Marine silt							
TL	9	3.53	109.92	1.51	559.12	557.61	188.23
DTLB	8	5.30	232.24	4.20	864.32	860.12	304.00
TTP	1	–	230.04	230.04	230.04	0.00	0.00
TV	0	–	0.00	0.00	0.00	0.00	0.00
DP	0	–	0.00	0.00	0.00	0.00	0.00
BS	1	2.51	4.69	4.69	4.69	0.00	0.00
Total #	19 (Currently active = 11, Currently inactive = 8)						
Marine sand							
TL	54	2.54	33.09	0.11	488.13	488.03	81.98
DTLB	72	5.01	58.89	0.29	635.03	634.74	101.52
TTP	266	–	4.50	0.00	181.03	181.03	15.34
TV	15	6.07	18.35	3.84	77.65	73.81	18.46
DP	55	1.67	0.36	0.00	4.10	4.10	0.56
BS	10	8.08	11.57	1.29	26.53	25.23	9.35
Total #	472 (Currently active = 345, Currently inactive = 127)						
Aolian sand							
TL	55.00	7.00	37.80	0.44	245.25	244.81	54.55
DTLB	65.00	8.87	37.26	0.02	239.17	239.15	46.26
TTP	168.00	–	1.86	0.00	24.67	24.66	3.23
TV	14.00	7.25	4.96	0.45	18.66	18.21	4.87
DP	35.00	2.36	0.64	0.04	4.06	4.02	0.74
BS	10.00	10.31	2.79	0.08	4.96	4.88	1.93
Total #	347 (Currently active = 247, Currently inactive = 100)						
Aolian silt							
TL	24.00	11.00	12.27	1.17	78.03	76.86	20.13
DTLB	23.00	19.26	80.22	1.01	321.05	320.04	86.02
TTP	341.00	–	1.21	0.00	59.48	59.48	5.68
AV	59.00	17.46	11.89	0.00	62.27	62.26	13.62
DP	0.00	–	0.00	0.00	0.00	0.00	0.00
BS	4.00	14.19	6.60	1.26	13.82	12.55	5.25
Total #	451 (Currently active = 428, Currently inactive = 23)						
Glacial drift and till							
TL	35.00	13.69	8.77	1.08	130.99	130.90	22.23
DTLB	0.00	–	0.00	0.00	0.00	0.00	0.00
TTP	0.00	–	0.00	0.00	0.00	0.00	0.00
TV	0.00	–	0.00	0.00	0.00	0.00	0.00
DP	0.00	–	0.00	0.00	0.00	0.00	0.00
BS	12.00	13.19	1.86	0.17	8.08	7.91	2.16
RTS	2.00	–	2.77	1.37	4.18	2.81	1.99
Total #	49 (Currently active = 47, Currently inactive = 2)						

Predicting the future responses of permafrost landscapes to warming is particularly challenging in areas already possessing complex thermokarst geomorphology. Different thermokarst landforms have varying mechanisms of thaw; hence different processes and rates can drive future topographic changes. Using diversity and density of landforms as indicators of landscape complexity reveals that areas underlain by aeolian silt are the most complex in terms of thermokarst geomorphology (Fig. 7). These areas exhibit a high density of landforms (21.8 per km^2) and a high diversity, with five different types of thermokarst landforms present. Areas underlain by marine silt are the least complex, with low landform density (0.8 landforms per km^2; Fig. 7), mainly because of the predominance of large drained-lake basins (Fig. 4, Table 4). Areas with higher landform diversity will probably experience a more diverse array of geomorphological responses to disturbances related to warming climate. Assessing the vulnerability to future thaw in areas underlain by glacial drift and deltaic sands is particularly challenging. Areas of glacial drift possess heterogeneous cryolithology and excess-ice content because of the presence of buried glacial ice. The distribution of excess ice within areas of deltaic sands is similarly unpredictable.

6. Conclusions

Results of this study improve understanding of future geomorphological responses to climate change in permafrost landscapes underlain by different surficial geologies in Arctic Alaska. Some of these results are also relevant to the ice-rich, coastal lowlands of northeast Siberia. Thermokarst landforms are widespread in Arctic Alaska and cover 60% of the 300-km^2 area we mapped. Some of these landforms are actively forming today, while others are relict features. Thermokarst-lakes and drained thermokarst-lake basins comprise the majority of thermokarst-affected terrain. Alas and thaw valleys and thermokarst troughs and pits are also widespread but occur at low densities. Permafrost temperatures are currently rising throughout Arctic Alaska, and widespread geomorphic changes related to permafrost thaw seem inevitable. Areas of marine silt are highly vulnerable to future thaw because they tend to be ice rich in their near surface sediments. However, because extensive thermokarst has already occurred in this surficial geology type over the course of the Holocene, these areas contain only limited amounts of excess ice in their upper few meters of sediment. The most severe thermokarst will probably occur in areas of aeolian silt (yedoma) because large expanses of these surficial geology types have not been previously disturbed by thaw (42% of total), and they contain large amounts of ice in deep, syngenetic ice-wedges formed during the coldest parts of the ice age.

Acknowledgements

LMF thanks the Arctic Landscape Conservation Cooperative and USGS Alaska Climate Science Center-funded Alaska Integrated Ecosystem Model Project for support. GG was supported by ERC #338335. DHM was partially supported by NSF grants ARC-0902169 and PLR-1417611.

Support for BMJ was provided by the USGS Land Change Science Program and Land Remote Sensing Program. The Teshekpuk Lake Observatory was critical for field support. We thank Reginald Muskett for assistance with permafrost temperature data, and Helene Genet for helpful conversations that improved the paper. We would like to thank the editor Richard Marston, Mikhail Kanevskiy, and three anonymous reviewers whose comments and suggestions greatly improved the manuscript. Any use of trade, product, or firm names is for descriptive purposes only and does not imply endorsement by the U.S. Government. Field logistics were provided in part by grants from the Bureau of Land Management and the National Science Foundation (NSF-PLR 1417611).

Appendix A

Table A.1
Study area metadata.

Site	Physiography	Surficial geology	Landform	Massive ice (% by volume) (Jorgenson et al., 2008a, 2008b)	Segregated ice (% by volume) (Jorgenson et al., 2008a, 2008b)	Total volumetric ice (%) (Kanevskiy et al., 2013)	Center of latitude (°N)	Center of longitude (°W)
A	Floodplain delta	Deltaic sands and gravels	Peaty, silty, fluvial + sandy coastal	10–30	≥50	73	70.7646°	−154.4776°
B	Coastal plain	Marine silt	Peaty silty lowland	10–30	≥50	86	70.7916°	−153.5925°
C	Coastal plain	Marine sand	Peaty sandy lowland	10–30	≥50	80	70.2055°	−151.4040°
D	Coastal plain	Marine sand	Peaty sandy lowland	10–30	≥50	80	70.7915°	−156.9147°
E	Coastal plain	Marine sand	Peaty sandy lowland	10–30	≥50	80	70.6474°	−157.8963°
F	Coastal plain	Marine sand	Peaty sandy lowland	10–30	≥50	80	70.3132°	−157.8071°
G	Coastal plain	Aeolian sand	Sandy lowland	5–10	<50	43	69.9295°	−153.0141°
H	Coastal plain	Aeolian sand	Sandy lowland	5–10	<50	43	70.2971°	−156.6817°
I	Coastal plain	Aeolian sand	Sandy lowland	5–10	<50	43	70.0339°	−153.9412°
J	Coastal plain	Aeolian silt	Silty lowland	30–70	≥50	89	69.9140°	−156.6158°
K	Upland	Aeolian silt	Silty upland	30–70	≥50	89	39.3271°	−152.0796°
L	Glaciated upland	Glacial drift	Rocky glacial upland	10–80	<50	no data	68.9769°	−149.8352°

Table A.2
Locations of permafrost boreholes used in this study.

Site	Latitude N	Longitude
Galbraith	68.479717°	−149.488767°
Inigok	69.989617°	−153.093833°
Umiat	69.395683°	−152.142800°
Koluktak	69.751600°	−154.617567°
Fish Creek	70.335233°	−152.052000°
South Meade	70.628467°	−156.835317°
Drew Point	70.864509°	−153.906745°

Table A.3
Slope statistics for each surficial geology region calculated using the Scenarios Network for Alaska (SNAP) 1 km resolution Alaska slope model (http://ckan.snap.uaf.edu/dataset/slope).

	Regional slope (°)			Mapped area slope (°)		
	Mean	Min	Max	Mean	Min	Max
Marine sand	0.10	0.00	1.24	0.06	0.01	0.12
Marine silt	0.03	0.00	0.11	0.04	0.02	0.06
Aeolian sand	0.10	0.00	0.71	0.06	0.01	0.14
Aeolian silt	0.32	0.00	1.80	0.27	0.05	0.70
Deltaic sands and gravels	0.04	0.00	0.21	0.01	0.00	0.02
Glacial drift	2.04	0.00	12.57	0.81	0.17	1.36

Appendix B

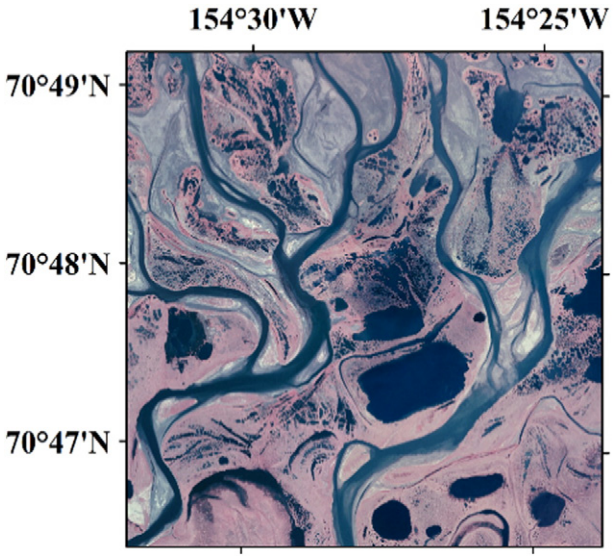

Fig. B1. Study area A.

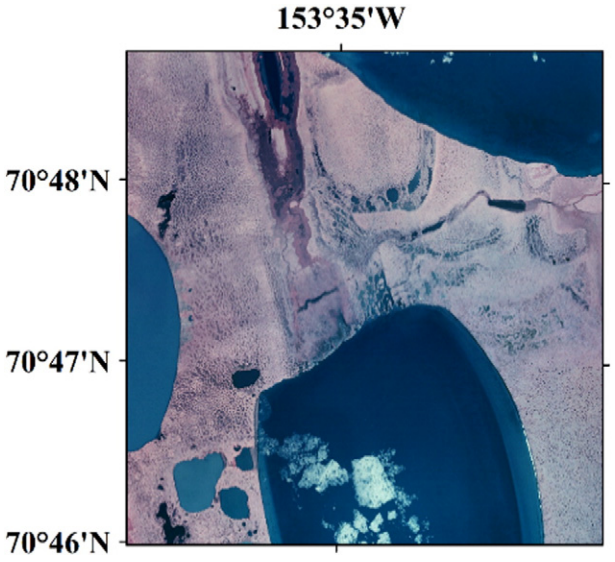

Fig. B2. Study area B.

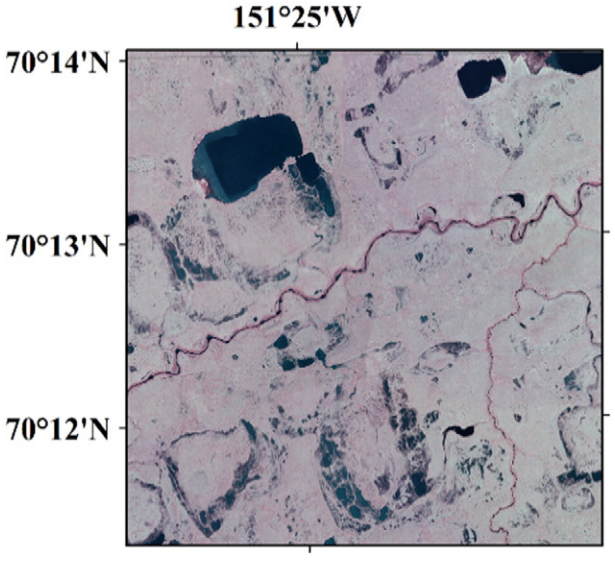

Fig. B3. Study area C.

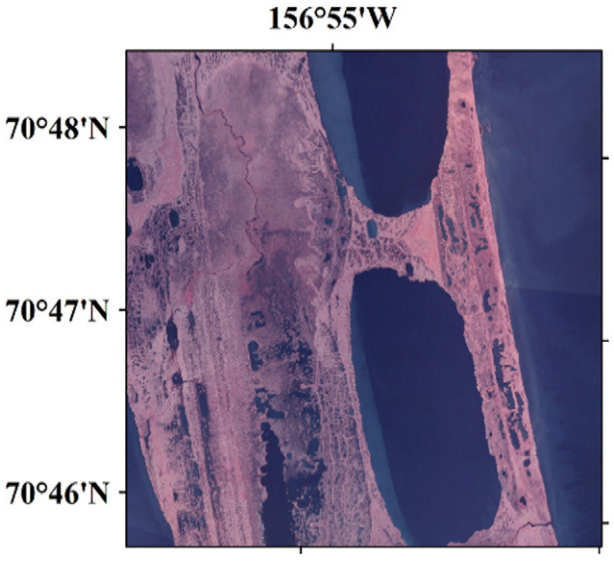

Fig. B4. Study area D.

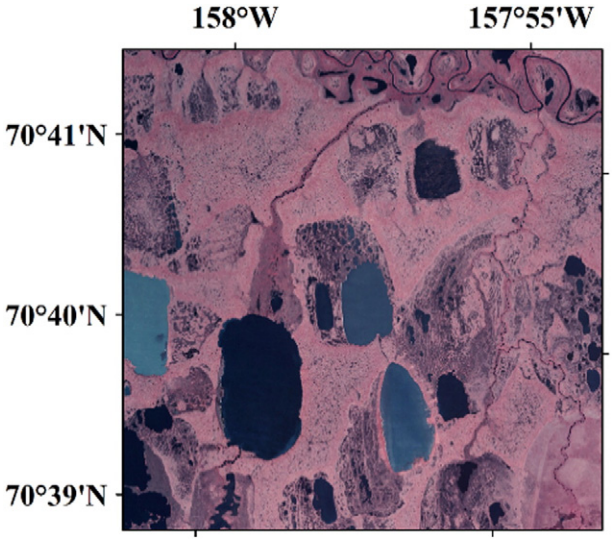

Fig. B5. Study area E.

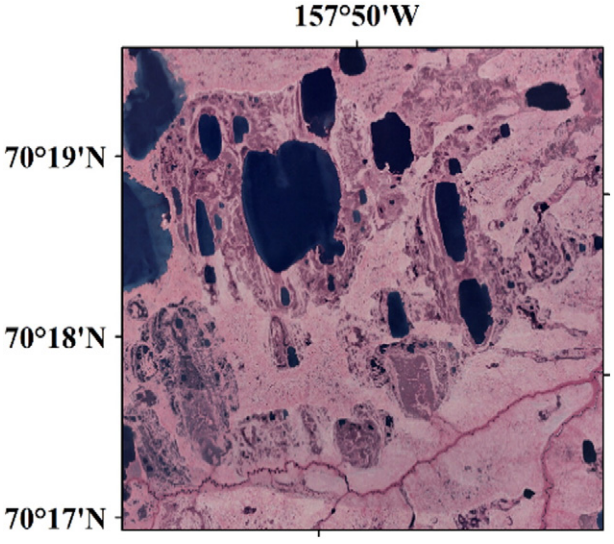

Fig. B6. Study area F.

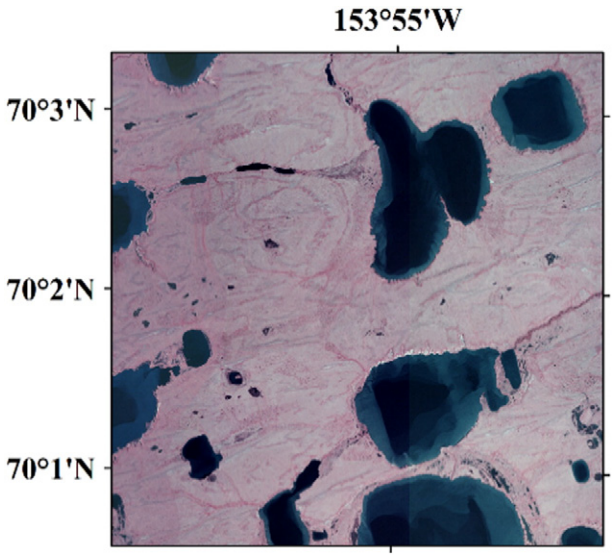

Fig. B7. Study area G.

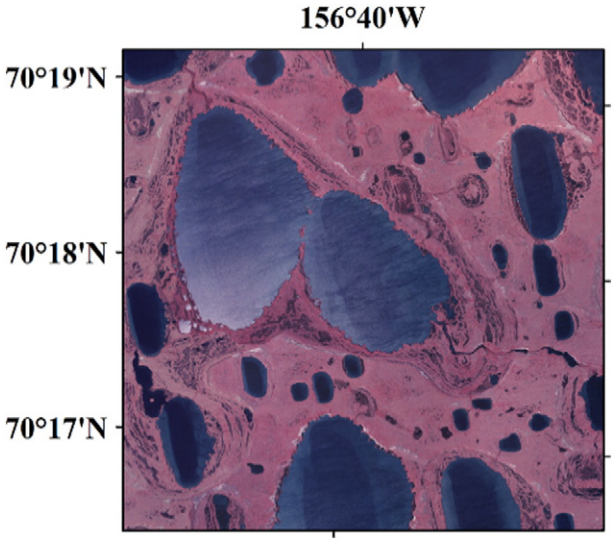

Fig. B8. Study area H.

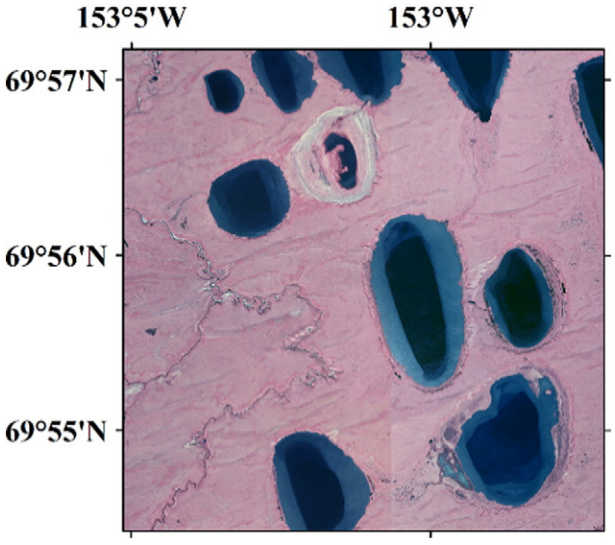

Fig. B9. Study area I.

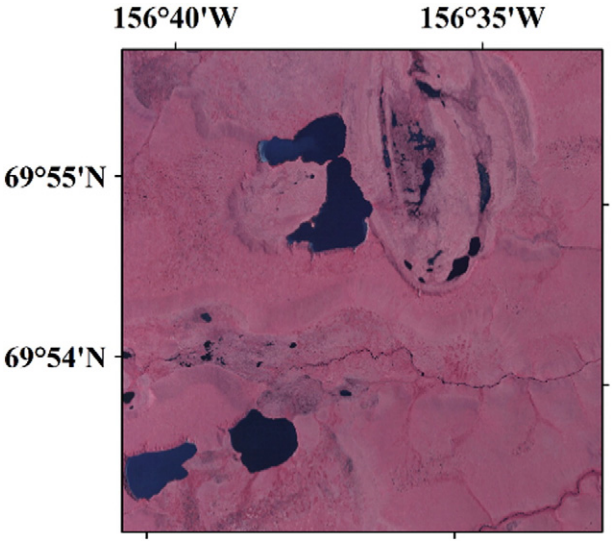

Fig. B10. Study area J.

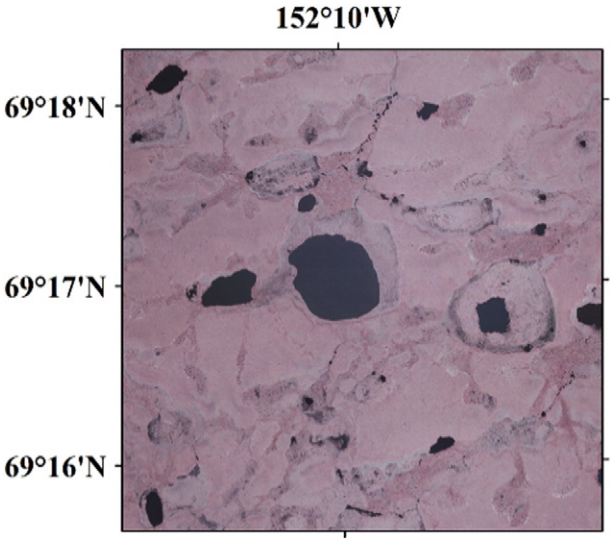

Fig. B11. Study area K.

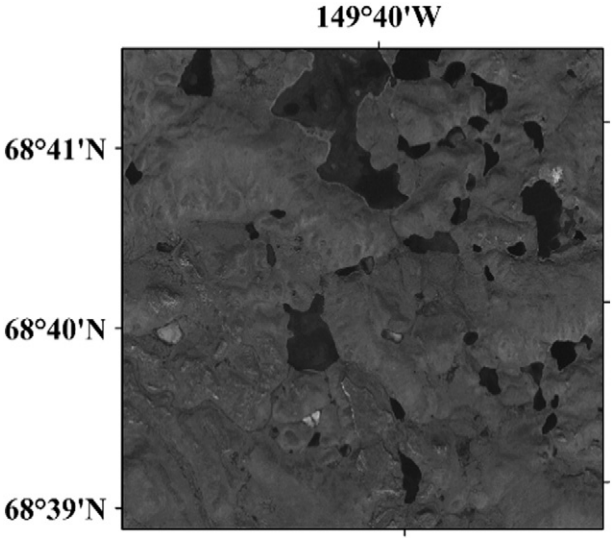

Fig. B12. Study area L.

References

Are, F.E., 1978. The reworking of shorelines in the permafrost zone. Proceedings of the Second International Conference on Permafrost, USSR Contribution. US National Academy of Sciences, Washington, DC, pp. 59–62.

Arp, C.D., Jones, B.M., 2009. Geography of Alaska lake districts: identification, description, and analysis of lake-rich regions of a diverse and dynamic state. US Geol. Surv. Sci. Investig. Rep. 2008–5215, 40.

Arp, C.D., Whitman, M.S., Jones, B.M., Grosse, G., Gaglioti, B.V., Heim, K.C., 2015. Distribution and biophysical processes of beaded streams in Arctic permafrost landscapes. Biogeosciences 12, 29–47.

Balser, A.W., Jones, J.B., Gens, R., 2014. Timing of retrogressive thaw slump initiation in the Noatak Basin, northwest Alaska, USA. J. Geophys. Res. Earth Surf. 119, 1106–1120.

Baughman, C.A., Mann, D.H., Verbyla, D.L., Kunz, M.L., 2015. Soil-surface organic layers in Arctic Alaska: spatial distribution, rates of formation, microclimatic effects. J. Geophys. Res. Biogeosci. 120, 1150–1164.

Billings, W.D., Peterson, K.M., 1980. Vegetational change and ice-wedge polygons through the thermokarst-lake cycle in Arctic Alaska. Arct. Alp. Res. 413–432.

Burn, C.R., 1992. Thermokarst-lakes. Can. Geogr. 36, 81–85.

Burn, C.R., Lewkowicz, A.G., 1990. Retrogressive thaw slumps. Can. Geogr. 34, 273–276.

Carter, L.D., 1981. A Pleistocene sand sea on the Alaskan arctic coastal plain. Science 211, 381–383.

Cohen, J., Screen, J.A., Furtado, J.C., Barlow, M., Whittleston, D., Coumou, D., Francis, J., Dethloff, K., Entekhabi, D., Overland, J., Jones, J., 2014. Recent Arctic amplification and extreme mid-latitude weather. Nat. Geosci. 7, 627–637.

Côté, M.M., Burn, C.R., 2002. The oriented lakes of Tuktoyaktuk Peninsula, western arctic coast, Canada: a GIS-based analysis. Permafr. Periglac. Process. 13, 61–70.

Czudek, T., Demek, J., 1970. Thermokarst in Siberia and its influence on the development of lowland relief. Quat. Res. 1, 103–120.

Dinter, D.A., Carter, L.D., Brigham-Grette, J., 1990. Late Cenozoic geologic evolution of the Alaskan North Slope and adjacent continental shelves. The Arctic Ocean Region. The Geology of North America 50, pp. 459–489.

Farquharson, L.M., Anthony, K.W., Bigelow, N., Edwards, M., Grosse, G., 2016. Facies analysis of yedoma thermokarst-lakes on the northern Seward Peninsula, Alaska. Sediment. Geol. 340, 25–37.

French, H.M., 2007. The Periglacial Environment. John Wiley and Sons (370 pp.).

French, H.M., Shur, Y., 2010. The principles of cryostratigraphy. Earth Sci. Rev. 101, 190–206.

Frohn, R.C., Hinkel, K.M., Eisner, W.R., 2005. Satellite remote sensing classification of thaw lakes and drained thaw lake basins on the North Slope of Alaska. Remote Sens. Environ. 97, 116–126.

Gaglioti, B.V., Mann, D.H., Jones, B.M., Pohlman, J.W., Kunz, M.L., Wooller, M.J., 2014. Radiocarbon age-offsets in an arctic lake reveal the long-term response of permafrost carbon to climate change. J. Geophys. Res. Biogeosci. 119, 557–566.

Galloway, J.P., Carter, D.L., 1993. Late Holocene longitudinal and parabolic dunes in arctic Alaska: preliminary interpretations of age and paleoclimatic significance. U.S. Geol. Surv. Bull. 2068, 3–11.

Goudie, A., 2004. Encyclopedia of Geomorphology. vol. 2. Psychology Press (1200 pp.).

Grosse, G., Schirrmeister, L., Kunitsky, V.V., Hubberten, H.W., 2005. The use of CORONA images in remote sensing of periglacial geomorphology: an illustration from the NE Siberian coast. Permafr. Periglac. Process. 16, 163–172.

Grosse, G., Schirrmeister, L., Malthus, T.J., 2006. Application of Landsat-7 satellite data and a DEM for the quantification of thermokarst-affected terrain types in the periglacial Lena-Anabar coastal lowland. Polar Res. 25, 51–67.

Grosse, G., Romanovsky, V.E., Walter, K., Morgenstern, A., Lantuit, H., Zimov, S.A., 2008. Distribution of thermokarst lakes and ponds at Three Yedoma Sites in Siberia. Ninth International Conferencnce on Permafrost. Institute of Northern Engineering, University of Alaska Fairbanks, Fairbanks, USA, pp. 551–556.

Grosse, G., Harden, J., Turetsky, M., McGuire, A.D., Camill, P., Tarnocai, C., Frolking, S., Schuur, E.A.G., Jorgenson, T., Marchenko, S., 2011. Vulnerability of high-latitude soil organic carbon in North America to disturbance. J. Geophys. Res. 116, G00K06.

Grosse, G., Jones, B., Arp, C., 2013. Thermokarst-lakes, drainage, and drained basins. In: Shroner Giardino, R., Harbor, J. (Eds.), Treatise on Geomorphology. Academic Press, San Diego, CA, pp. 325–353.

Hamilton, T.D., 2003. Glacial geology of the Toolik Lake and upper Kuparuk River regions. In: Walker, D.A. (Ed.), Biological Papers of the University of Alaska, p. 24.

Hinkel, K.M., Eisner, W.R., Bockheim, J.G., Nelson, F.E., Peterson, K.M., Dai, X., 2003. Spatial extent, age, and carbon stocks in drained thaw lake basins on the Barrow Peninsula, Alaska. Arct. Antarct. Alp. Res. 35, 291–300.

Hinkel, K.M., Frohn, R.C., Nelson, F.E., Eisner, W.R., Beck, R.A., 2005. Morphometric and spatial analysis of thaw lakes and drained thaw lake basins in the western Arctic Coastal Plain, Alaska. Permafr. Periglac. Process. 16, 327–341.

Homer, C.G., Dewitz, J.A., Yang, L., Jin, S., Danielson, P., Xian, G., Coulston, J., Herold, N.D., Wickham, J.D., Megown, K., 2015. Completion of the 2011 National Land Cover Database for the conterminous United States-representing a decade of land cover change information. Photogramm. Eng. Remote Sens. 81, 345–354.

Hu, F.S., Higuera, P.E., Duffy, P., Chipman, M.L., Rocha, A.V., Young, A.M., Kelly, R., Dietze, M.C., 2015. Arctic tundra fires: natural variability and responses to climate change. Front. Ecol. Environ. 13, 369–377.

Intermap, 2010. Product Handbook and Quick Start Guide, Standard Edition. Intermap, p. v 4.4.

IPCC, 2013. Climate change 2013: the physical science basis. Intergov. Panel Clim. Chang.

Jones, B.M., Arp, C.D., 2015. Observing a catastrophic thermokarst lake drainage in Arctic Alaska. Permafr. Periglac. Process. 26, 119–128.

Jones, B.M., Grosse, G., Arp, C.D., Jones, M.C., Walter Anthony, K., Romanovsky, V.E., 2011. Modern thermokarst-lake dynamics in the continuous permafrost zone, northern Seward Peninsula, Alaska. J. Geophys. Res. 116, 2005–2012.

Jones, M.C., Grosse, G., Jones, B.M., Walter Anthony, K.M., 2012. Peat accumulation in a thermokarst-affected landscape in continuous ice-rich permafrost, Seward Peninsula, Alaska. J. Geophys. Res. Biogeosci. 117 (G2).

Jones, B.M., Grosse, G., Arp, C.D., Miller, E., Liu, L., Hayes, D.J., Larsen, C.F., 2015. Recent Arctic tundra fire initiates widespread thermokarst development. Sci. Rep. 5, 15865.

Jorgenson, M.T., 2013. Thermokarst terrains. In: Shroder, J.F., Giardino, R., Harbor, J. (Eds.), Treatise on Geomorphology, Vol 8, Glacial and Periglacial Geomorphology. Academic Press, San Diego, pp. 313–324 (Vol. Eds.).

Jorgenson, M.T., Shur, Y., 2007. Evolution of lakes and basins in arctic Alaska and discussion of the thaw lake cycle. J. Geophys. Res. Earth Surf. 112 (F2).

Jorgenson, M.T., Shur, Y.L., Walker, H.J., 1998. Evolution of a permafrost-dominated landscape on the Colville River Delta, northern Alaska. In: Lewkowicz, A.G., Allard, M. (Eds.), Seventh International Conference on Permafrost. Collection Nordica, Yellowknife, Canada, pp. 523–529.

Jorgenson, M.T., Shur, Y.L., Pullman, E.R., 2006. Abrupt increase in permafrost degradation in Arctic Alaska. Geophys. Res. Lett. 33.

Jorgenson, M.T., Shur, Y.L., Osterkamp, T.E., 2008a. Thermokarst in Alaska. In: Kane, D.L., Hinkel (Eds.), Ninth International Conference on Permafrost. Institute of Northern Engineering, University of Alaska Fairbanks, Fairbanks, Alaska, pp. 869–876.

Jorgenson, M.T., Yoshikawa, K., Kanevskiy, M., Shur, Y., Romanovsky, V.E., Marchenko, S., Grosse, G., Brown, J., Jones, B., 2008b. Permafrost characteristics of Alaska – a new permafrost map of Alaska. In: Kane, D.L., Hinkel, K.M. (Eds.), Ninth International Conference on Permafrost. Institute of Northern Engineering, University of Alaska Fairbanks, Fairbanks, Alaska, pp. 551–556.

Jorgenson, T., Kanevskiy, M.Z., Shur, Y., Moskalenko, N.G., Brown, D.R.N., Wickland, K., Striegl, R., Koch, J., 2015. Ground ice dynamics and ecological feedbacks control ice-wedge degradation and stabilization. JGR Earth Surf. 120 (11), 2280–2297.

Kanevskiy, M., Shur, Y., Fortier, D., Jorgenson, M.T., Stephani, E., 2011. Cryostratigraphy of late Pleistocene syngenetic permafrost (yedoma) in arctic Alaska, Itkillik River exposure. Quat. Res. 75, 584–596.

Kanevskiy, M., Shur, Y., Jorgenson, M.T., Ping, C.L., Michaelson, G.J., Fortier, D., Stephani, E., Dillon, M., Tumskoy, V., 2013. Ground ice in the upper permafrost of the Beaufort Sea coast of Alaska. Cold Reg. Sci. Technol. 85, 56–70.

Kokelj, S.V., Jorgenson, M.T., 2013. Advances in thermokarst research. Permafr. Periglac. Process. 24, 108–119.

Kokelj, S.V., Jenkins, R.E., Milburn, D., Milburn, D., Burn, C.R., Snow, N.B., Burn, C.R., Snow, N., 2005. The influence of thermokarst disturbance on the water quality of small upland lakes, Mackenzie Delta region, Northwest Territories, Canada. Permafr. Periglac. Process. 16, 343–353.

Kokelj, S.V., Lantz, T.C., Kanigan, J., Smith, S.L., Coutts, R., 2009. Origin and polycyclic behaviour of tundra thaw slumps, Mackenzie Delta region, Northwest Territories, Canada. Permafr. Periglac. Process. 20, 173–184.

Lamoureux, S.F., Lafreniére, M.J., 2009. Fluvial impact of extensive active layer detachments, Cape Bounty, Melville Island, Canada. Arct. Antarct. Alp. Res. 41, 59–68.

Lantuit, H., Pollard, W.H., 2008. Fifty years of coastal erosion and retrogressive thaw slump activity on Herschel Island, southern Beaufort Sea, Yukon Territory, Canada. Geomorphology 95, 84–102.

Lantz, T.C., Kokelj, S.V., 2008. Increasing rates of retrogressive thaw slump activity in the Mackenzie Delta region, N.W.T., Canada. Geophys. Res. Lett. 35, 1–5.

Lewkowicz, A.G., Harris, C., 2005. Morphology and geotechnique of active-layer detachment failures in discontinuous and continuous permafrost, northern Canada. Geomorphology 69, 275–297.

Liljedahl, A.K., Boike, J., Daanen, R.P., Fedorov, A.N., Frost, G.V., Grosse, G., Hinzman, L.D., Iijma, Y., Jorgenson, J.C., Matveyeva, N., Necsoiu, M., Raynolds, M.K., Romanovsky, V., Schulla, J., Tape, K.D., Walker, D.A., Wilson, C., Yabuki, H., Zona, D., 2016. Pan-Arctic ice-wedge degradation in warming permafrost and influence on tundra hydrology. Nat. Geosci. 9, 312–318.

Macdonald, G.M., Beilman, D.W., Kremenetski, K.V., Sheng, Y., Smith, L.C., Velichko, A.A., 2006. Rapid early development of circumarctic peatlands and atmospheric CH_4 and CO_2 variations. Science 314, 285–288.

Mack, M.C., Bret-Harte, M.S., Hollingsworth, T.N., Jandt, R.R., Schuur, E.A., Shaver, G.R., Verbyla, D.L., 2011. Carbon loss from an unprecedented Arctic tundra wildfire. Nature 475 (7357), 489–492.

Mann, D.H., Peteet, D.M., Reanier, R.E., Kunz, M.L., 2002. Responses of an arctic landscape to lateglacial and early holocene climatic changes: the importance of moisture. Quat. Sci. Rev. 21, 997–1021.

Mann, D.H., Groves, P., Reanier, R.E., Kunz, M.L., 2010. Floodplains, permafrost, cottonwood trees, and peat: what happened the last time climate warmed suddenly in arctic Alaska? Quat. Sci. Rev. 29, 3812–3830.

Morgenstern, A., Grosse, G., Günther, F., Fedorova, I., Schirrmeister, L., 2011. Spatial analyses of thermokarst-lakes and basins in Yedoma landscapes of the Lena Delta. Cryosphere 5, 849–867.

Myers-Smith, I.H., Harden, J.W., Wilmking, M., Fuller, C.C., McGuire, A.D., Chapin III, F.S., 2007. Wetland succession in a permafrost collapse: interactions between fire and thermokarst. Biogeosci. Discuss. 4 (6), 4507–4538.

Olthof, I., Fraser, R.H., Schmitt, C., 2015. Landsat-based mapping of thermokarst-lake dynamics on the Tuktoyaktuk Coastal Plain, Northwest Territories, Canada since 1985. Remote Sens. Environ. 168, 194–204.

Raynolds, M.K., Walker, D.A., Maier, H.A., 2006. Alaska Arctic Tundra Vegetation Map. Scale 1:4,000,000. Conservation of Arctic Flora and Fauna Map.

Raynolds, M.K., Walker, D.A., Ambrosius, K.J., Brown, J., Everett, K.R., Kanevskiy, M., Kofinas, G.P., Romanovsky, V.E., Shur, Y., Webber, P.J., 2014. Cumulative geoecological effects of 62 years of infrastructure and climate change in ice-rich permafrost landscapes, Prudhoe Bay Oilfield, Alaska. Glob. Chang. Biol. 20, 1211–1224.

Romanovsky, V.E., Smith, S.L., Christiansen, H.H., 2010. Permafrost thermal state in the polar northern hemisphere during the international polar year 2007–2009: a synthesis. Permafr. Periglac. Process. 21, 106–116.
Romanovsky, V.E., Smith, S.L., Christiansen, H.H., Shiklomanov, N.I., Streletskiy, D.A., Drozdov, D.S., Malkova, G.V., Oberman, N.G., Kholodov, A.L., Marchenko, S.S., 2015. Terrestrial Permafrost (in "State of the Climate in 2014"). Bull. Am. Meteorol. Soc. 96 (7), S139–S141.
Schirrmeister, L., Froese, D., Tumskoy, V., Grosse, G., Wetterich, S., 2013. Yedoma: Late Pleistocene ice-rich syngenetic permafrost of Beringia. Encyclopedia of Quaternary science. 2nd edition. In: Elias, S., Mock, C., Murton, J. (Eds.), Encyclopedia of Quaternary Science, second ed. Elsevier, Amsterdam, pp. 542–552 (3888 pp.).
Shur, Y., Kanevskiy, M., Jorgenson, T., Dillon, M., Stephani, E., Bray, M., 2012. Permafrost degradation and thaw settlement under lakes in yedoma environment. In: Hinkel, K.M. (Ed.), Tenth International Conference on Permafrost Salekhard, Russia.
Shur, Y.L., Jorgenson, M.T., 1998. Cryostructure development on the floodplain of the Colville River Delta, Arctic Alaska. In: Lewkowicz, A.G., Allard, M. (Eds.), Seventh International Conference on Permafrost. Collection Nordica, Yellowknife, Canada.
Smith, S.L., Romanovsky, V.E., Lewkowicz, A.G., Burn, C.R., Allard, M., Clow, G.D., Yoshikawa, K., Throop, J., 2010. Thermal state of permafrost in North America: a contribution to the International Polar Year. Permafr. Periglac. Process. 21, 117–135.
Soloviev, P.A., 1973. Thermokarst phenomena and landforms due to frost heaving in central Yakutia. Builetyn Perglacjalny 23, 135–155.
Steedman, A.E., Lantz, T.C., Kokelj, S.V., 2016. Spatio-temporal variation in high-centre polygons and Ice-Wedge Melt Ponds, Tuktoyaktuk Coastlands, Northwest Territories. Permafr. Periglac. Process.
van Everdingen, R., 2005. Multi-language Glossary of Permafrost and Related Ground-ice Terms. Natl. Snow Ice Data Center/World Data Cent. Glaciol., Boulder.
Veremeeva, A., Gubin, S., 2009. Modern tundra landscapes of the Kolyma Lowland and their evolution in the Holocene. Permafr. Periglac. Process. 20 (4), 399–406.
Wahrhaftig, C., 1965. Physiographic Divisions of Alaska, Geological Survey Professional Paper 482.
Wang, J., Sheng, Y., Hinkel, K.M., Lyons, E.A., 2012. Drained thaw lake basin recovery on the western Arctic Coastal Plain of Alaska using high-resolution digital elevation models and remote sensing imagery. Remote Sens. Environ. 119, 325–336.
Washburn, A.L., 1979. Geocryology: A Survey of Periglacial Processes and Environments. Edward Arnold, London (416 pp.).
Wendler, G., Shulski, M., Moore, B., 2010. Changes in the climate of the Alaskan North Slope and the ice concentration of the adjacent Beaufort Sea. Theor. Appl. Climatol. 99, 67–74.
Yershov, E.D., 1998. General Geocryology. Cambridge University Press, Cambridge (580 pp.).